Augmentation of Onboard Camera Data with Vessel Manoeuvrability for Tactical Navigational Support Analysis

By

Mordecai Benny Chimedza

A thesis submitted to the

School of Graduate Studies

In partial fulfillment of the requirements for the degree of

Master of Engineering

Faculty of Engineering and Applied Science

MEMORIAL UNIVERSITY

May 2025

St. John's Newfoundland and Labrador

Abstract

Shipping in Canadian Arctic waters involves significant risks, primarily due to potential ice interactions. To address these challenges, various support tools have been developed to enhance safe navigation in ice-prone regions. These include POLARIS, a system which evaluates vessel suitability for specific ice conditions, and onboard cameras, which act as sensors to capture and monitor ice conditions around a vessel. This study examines the effectiveness of these two decision support tools, emphasizing the need to account for operational parameters such as vessel speed and physical characteristics like vessel length when assessing a ship's ability to navigate safely through ice.

Image processing techniques, including projective transformation, are applied to convert onboard camera data into a top-down view, enabling augmentation of ship manoeuvrability parameters stopping distance and turning circle. Image rescaling is further employed to achieve a true-scale representation of distances within the field of view. Two sample vessels are analyzed to evaluate their manoeuvrability in a test case involving a 50m diameter ice hazard at 175m directly ahead of the vessel. The results demonstrate the critical role of vessel speed in stopping distance and vessel length in the turning circle. The results also show the limitations of using onboard cameras for tactical navigational support, as well as highlighting the limits that POLARIS has in terms of accounting for differences in vessels within the same ice class but with different capabilities.

Acknowledgements

I would like to sincerely thank my co-supervisors, Dr. Rocky Taylor and Dr. Thomas Browne, for their invaluable guidance and support in shaping the direction of this research. I would also like to acknowledge Dr. Ian Turnbull and Dr. Oscar Desilva for their insights on specific aspects of the project.

Moreover, I am grateful to Memorial University of Newfoundland, the National Research Council of Canada (NRC), the Natural Sciences and Engineering Research Council (NSERC) and the Hibernia Management and Development Company (HMDC) for their financial support. I further acknowledge the NRC for providing the data that was essential to this work.

Finally, I wish to extend my heartfelt appreciation to my friends and family, whose unwavering encouragement has sustained me throughout this research journey. Believing that good things take time, I hope that the extended duration of this research process has resulted in a product of corresponding quality

Table of Contents

List of Figures

List of Tables

List of Abbreviation

POLARIS	- Polar Operational Limit Assessment Risk Indexing System
IACS	- International Association of Classification Society
CIS	- Canadian Ice Service
WMO	- World Meteorological Organization
IMO	- International Maritime Organization
LiDAR	- Light Detection and Ranging
ASMR	- Advanced Microwave Scanning Radiometer
SAR	- Synthetic Aperture Radar
UAV	- Unmanned Aerial Vehicle
ZDS	- Zone Date System
AIRSS	- Arctic Ice Regime Shipping System
ASPPR	- Arctic Shipping Pollution Prevention Regulations
RIV	- Risk Index Values
RIO	- Risk Index Outcome
PC	- Polar Class
ABS	- American Bureau of Shipping
VLCC	- Very Large Crude Carrier
CFD	- Computational Fluid Dynamics
CCGS	- Canadian Coast Guard Ship
MCR	- Maximum Continuous Rating
BHP	- Brake Horse-Power
RPM	- Revolutions Per Minute

Chapter 1: Introduction

1.1.Overview

Operating vessels in the Canadian Arctic has long been a challenging task due to the risk of ice hazards. To reduce this risk, decision support tools have been developed to facilitate safe navigation. Among these tools is the use of onboard cameras for gathering data on sea ice conditions, which is useful for the real time tactical navigation decision making support. This study evaluates the effectiveness of such onboard visual systems by integrating their data with vessel capabilities and operational guidelines from the POLARIS support tool, highlighting both the potential and limitations of these onboard camera systems.

This chapter provides an overview of the context, significance, and objectives of the study, Chapter 2 presents a review of the relevant literature. Chapter 3 details the methodologies used for the calculations and analyses. Chapter 4 presents the results, while Chapter 5 focuses on their analysis. Finally, Chapter 6 outlines the conclusions drawn from the study. An appendix is also included with the MATLAB code used to perform the calculations and image processing steps.

1.2.Problem Definition

Navigating ice-covered waters presents multiple risks, primarily the continuous need to monitor for ice hazards near the vessel. To mitigate these risks, several methods are employed. During voyage planning, seafarers use data such as ice charts, which provide a broad overview of ice features and sea ice coverage. These charts aid in route selection and help avoid areas with high ice concentrations. However, the marine environment is highly dynamic, with conditions constantly changing. Additionally, ice charts used for high-level planning have low spatial resolution and do not depict smaller ice hazards that pose localized threats. As a result, real-time tactical navigation is essential for continuously monitoring ice conditions around the vessel.

Tactical navigation relies primarily on lookouts who visually monitor ice conditions around the vessel. Recently, onboard cameras have been introduced to automate this process, with data analyzed to identify ice hazards.

The key question this research seeks to answer is how effectively these camera systems support vessel operations in practice—specifically, their ability to detect ice hazards in a timely manner and assist in hazard avoidance. The aims of the research are further expanded on in the next section outlining the objectives of this research work.

1.3.Project Objectives

This project aims to answer the research question by analyzing image data collected aboard the Canadian Coast Guard Ship (CCGS) Amundsen to evaluate its effectiveness as a proof of concept for using cameras in tactical ice navigation. The study incorporates the POLARIS framework, a regulatory guideline for vessel operations in ice-covered waters, to ensure alignment with industry standards. Specifically, this study seeks to achieve the following objectives:

a. Provide a visual representation and analysis of the vessel's hazard avoidance options based on POLARIS recommendations, which specify allowable speeds for different POLARIS vessel classifications.
b. Highlight the importance of considering vessel properties when assessing hazard avoidance capabilities. In this context, stopping distance and turning circle parameters are used to illustrate a vessel's maneuverability and options for avoiding ice hazards.

c. Assess the effectiveness of camera data for tactical navigation and hazard avoidance. This evaluation is based on an off-the-shelf camera system, specifically the Sony HDR-AS100V.

Chapter 2: Literature Review

2.1. Background on Shipping in Ice

The warming of the Arctic has created new opportunities for maritime traffic in Arctic waters [1] [2] [3] [4]. However, navigation in the polar regions is associated with various risks, particularly the potential of impact with icebergs and sea ice [5] [6] [3]. Additionally, there has been a drive to develop methods to support autonomous vessel navigation in ice conditions [7]. In view of this, several methods have been employed to mitigate and to actively manage the risks posed by ice, with ice monitoring being a key component [8] [9]. A key aspect of ice monitoring is the collection of information and the observing of ice conditions for tactical navigation decision support [10]. Methods such as LiDAR, satellite imagery and onboard human monitoring have been employed for navigation and path planning [11] [12] 13] 14].

Typically, operators onboard the vessel assess the ice environment to aid in real time decision-making on the path to follow [15]. This process involves assessing the ice regime surrounding the vessel, its stage of development and the concentration, as well as its proximity to the vessel and the risk level posed [15] [16]. To assist operators in assessing the immediate environment for sea ice and iceberg risk, the use of onboard cameras has been employed [17] [18] [19] [20].

Since onboard cameras are being deployed to aid with ice monitoring, it is necessary to assess and demonstrate how the information acquired through these systems is of practical value for tactical navigation support. This helps to inform the current efforts to integrate these systems in ice monitoring protocols. The objective of this thesis is to propose a method to process ship-based camera images and integrate ship manoeuvrability and ship operational limit guidelines to assess the utility of onboard cameras in supporting tactical navigation decision making.

A key regulatory guideline used to help guide navigation in ice regions is called POLARIS. POLARIS, which is an acronym for Polar Operational Limit Assessment Risk Indexing System, is a system used to assess the risk of operations given ice conditions and a vessel's ice class [21]. The vessel ice class or polar class is determined by the International Association of Classification Society (IACS) Polar Class system. While POLARIS is extremely useful, the limitations it has will be highlighted to depict the need to factor in other vessel parameters in assessing risk and options for ice hazard avoidance for a given vessel.

In the following section, the role of ice monitoring to support voyage planning and tactical navigation is introduced. Approaches for sea ice monitoring and their capabilities and limitations are reviewed, specifically remote sensing and onboard cameras.

2.2. Ice Monitoring for Vessels

There are three general approaches to dealing with ice for offshore vessels and structures: avoidance, usage or interaction, and elimination of the ice hazards [22]. The decision on which approach to use will depend on a range of factors including the vessel's capabilities, operational conditions, and ice characteristics [4]. This, therefore, creates a need for accurate ice detection and characterization in order to support vessels in real time to deal with potential hazards.

For sea ice, the characterization of the ice environment or the surrounding ice regime is performed by identifying the nature of the ice, including the concentration, and stage of development [22]. The stage of development is characterised by two attributes, an ice thickness range and its nominal age [22]. Sea ice concentration deals with the percentage of a given ocean area that is covered with sea ice. Lower concentrations may mean a possibility to employ avoidance strategies to ensure no contact of vessels with the ice. Higher concentrations typically imply inevitable ice interaction.

The organization responsible for providing ice information in Canada is the Canadian Ice Service (CIS). CIS has developed a system for describing ice regimes, using what is known as the Egg Code [22]. The Egg Code is a pictorial description of ice regime conditions. Figure 2.1 is an illustration of the Egg Code, along with explanations of the descriptive entries. Ice types are defined based on their stage of development considering ranges of ice thickness and nominal age, following the World Meteorological Organization's (WMO) nomenclature for sea ice. Partial concentrations are generally reported in tenths, e.g., 2/10th for 20% areal coverage of a given ice type or open water.

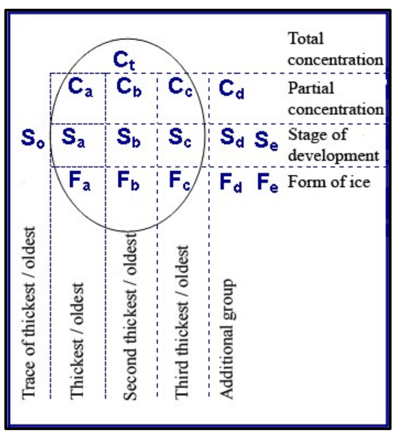

Figure 2.1 The Egg Code, a method used to describe ice regime by the CIS [22]

Usually, before a vessel goes on its voyage in polar regions, an optimal route is planned using the available strategic information provided by ice data sources such as CIS ice charts, as well as other relevant voyage planning information [23] [24] [16].

The voyage plan has to comply with the requirements of the International Maritime Organization's (IMO) Polar Code [25]. The Polar Code is a set of regulations that help to set the operational and environmental standards for polar shipping to ensure safe operations [26 [27]. Compliance with the code involves ensuring that a vessel's class designation matches the anticipated operational conditions, mostly the ice conditions [16]. Despite this initial planning, conditions have to be continually monitored throughout the voyage since the sea is a dynamic environment.

Most of the methods of ice monitoring mentioned in this chapter are useful for the initial voyage planning, but for real time continuous voyage planning, ice detection methods with a higher temporal and spatial scale are needed such as the use of onboard lookouts [28]. Onboard cameras have also shown potential in assisting this process of continuous path planning as they offer real time situational awareness of ice conditions and provide visual data that can be readily interpreted by a duty officer or crew on deck to make tactical navigational decisions [29]. This present work will seek to highlight the extent of the practical utility of onboard cameras.

2.2.1. Remote Sensing Methods

Remote sensing is another form of modern sea ice monitoring. The remote sensing methods are typically satellite based methods that can overcome cloud cover and adverse weather conditions to capture sea ice information. These methods have varying temporal and spatial scale resolutions and can characterize properties such as sea ice extent, thickness, concentration, and motion [12]. Some of the techniques used include Passive Microwave Radiometry, Synthetic Aperture Radar (SAR) and Light Detection And Ranging (LiDAR) [11] [30].

Passive Microwave Radiometry is used to detect sea ice extent, concentration, and thickness [11]. It is unaffected by cloud cover or the amount of daylight. Microwave satellite data has been used to collect passive information about sea ice extent from as far back as 1972. However, this monitoring method has proven that it is limited by its spatial resolution. This makes it less relevant for real time tactical navigation support [31] [32] [33]. The low spatial resolution means that ice features cannot be sufficiently characterised to inform tactical navigation decision-making [34]. For example, Advanced Microwave Scanning Radiometer for EOS (ASMR-E) gives data at the kilometer level of resolution [35].

Synthetic Aperture Radar (SAR) is a form of active microwave remote sensing which works by measuring the backscatter signal of its transmitted microwave pulses to provide high resolution images of sea ice morphology [36]. SAR is also used to produce sea ice charts which can be used to assess sea ice risk and support vessel route planning [37] [38] [16]. It provides data at spatial scales in the meter level which is more useful than the passive microwave methods [35].

The limitation of SAR is that the sensor data requires significant processing to provide information that can be interpreted for decision making [39]. Additionally, this method demands computationally intensive methods for the processing, making it an expensive option [28]. The high spatial scale has made the use of SAR valuable for strategic planning to sea-going vessels. However, for tactical planning, there is need for higher temporal resolutions, almost real time, which SAR cannot yet provide. This limitation in SAR data collection is often augmented by the use of personnel working onboard as lookouts for ice hazards. [40] [36].

Light Detection And Ranging (LiDAR) is used for ice information gathering. It is a form of remote sensing which is deployed on aircraft or Unmanned Aerial Vehicles (UAVs) [30]. It is used to measure the sea ice surface elevation and roughness with high precision [41] [42]. One of its clear limitations is that it requires deployment of a secondary vehicle, e.g. a drone, for information gathering. It also has limited spatial coverage since it has to pass over the region on which it is collecting information [30] [35]. Table 2.1 summarizes the discussed methods for remote ice monitoring for vessels.

Table 2.1 showing a summary of the capabilities of some of the technologies used for remote ice monitoring

Method	**Spatial Scale**	**Temporal Scale**	**Limitations**
Passive Microwave	5 - 50km	Daily to sub daily	Low spatial scale for ice feature info [43] [44] [45].
SAR	1 - 100m depends on mode and sensor	6-12 days with possible daily	Processing is computationally intensive [28]
LiDAR	cm to m	Per deployment	Limited by duration and coverage of data collection campaigns [46] [41].

2.2.2. In Situ Measurement Methods

In addition to remote sensing, in situ methods are used to provide ground truth validation of sea ice data. These provide information at a finer scale and can be in the form of the following: collection of ice cores, sonar sensors profiling ice features, deployment of underwater vessels with sensors attached, and deployment of buoys for ice tracking [47] [48] [49] [50]. Since in situ measurements are used for validation or ice property measurements and not for navigation or path planning, these methods won’t be discussed further in this present work.

2.2.3. Visual Systems

The remote ice monitoring and detection methods described previously have limitations in terms of limited spatial resolution or coverage. Where some have shown superior resolutions, they are not practical from a tactical navigational planning perspective due to high computational processing requirements (i.e., SAR) and limited spatial coverage (i.e., LiDAR). This has led to the adoption and advancement of visual based systems for navigation support.

The most basic visual method is the use of crew members to perform visual observations (lookouts) in the direction of the vessel's movement at various intervals [51]. The task of the lookouts is to detect and monitor for ice hazards such as icebergs and sea ice floes [52] [12]. These crew members evaluate ice conditions, which is a subjective practice as it depends on the individual and their experience and level of knowledge [53] [16].

Given the subjective nature of human observers, i.e. the interpretations of the same information can be different for different experts, it is useful to develop a system that can provide objective evaluations of ice conditions. Additionally, the number of people with experience is limited and thus personnel might not be available to be deployed on every vessel that will be traversing icy conditions. Thus, the process of tactical navigation support has recently been supported by the deployment of digital cameras, either onboard a vessel or on aerial vehicles or drones. The focus in this thesis is on the use of data from onboard camera systems. Such data is of high spatial and temporal resolution at near real time and thus provides significant benefits for real time tactical navigation support.

Several studies have shown the promise of onboard visual camera data. For example, Dowden et al 2021 makes use of images obtained onboard the Nathaniel B Palmer icebreaker to classify sea ice using a machine learning neural network with satisfactory results in detecting sea ice and in correctly classifying new gray and first year ice [54]. In another example, Wright et al 2017 demonstrates the potential of detection algorithms to classify the different ice features of sea ice, snow and melt ponds in the Arctic [55]. Zhou et al 2023 describes a method that uses a computer vision system called YOLOACT to determine sea ice concentration and floe size distribution accurately and automatically from optical imagery [12].

Panchi et al 2021 analyzes the performance of twelve different neural networks to classify optical imagery with varied success [56]. Peng Lu et al 2010 demonstrates the potential of using visual imagery onboard a ship to determine sea ice concentration after correcting for the geometric distortion of the images [57]. Zhang et al 2015 also explores the performance of an algorithm on identifying floe size distributions from the optical imagery that was obtained from an unmanned aerial vehicle [20].

The images used for analysis in this project were obtained from a vessel called the CCGS Amundsen, operating in sub-Arctic waters. The Amundsen vessel is a Canadian Coast Guard vessel which is used for various tasks including ice observation activities. The images were obtained from an onboard camera that was set up on the vessel bridge by the National Research Council of Canada. In Figure 2.2, the approximate position of the camera onboard the vessel is shown. Additionally, Figure 2.3 gives the camera's forward view.

Figure 2.1 The vessel and approximate location of the camera [58]

Figure 2.2 A sample visual of the vessel forward view

The objective of the current work is the development of a process for augmenting of the onboard visual camera data considering vessel manoeuvrability capabilities and the region of interest for navigation. Results provide insights to the efficacy and potential limitations of onboard camera systems for tactical navigation support.

2.3. Decision Support Tools for Ice Navigation

In addition to ice monitoring methods, there are also auxiliary tools and guidelines that are used to help navigation in ice conditions. These methods include POLARIS, the ZDS and AIRSS systems. These methods are explored in the following sections.

2.3.1. ZDS System

The ZDS system, which stands for Zone Date System, is one of the first methodologies that was used to provide support for vessel operations in the Canadian Arctic [59]. It was introduced under the Arctic Shipping Pollution Prevention Regulations (ASPPR) in 1972 [60]. The system assumes that nature follows a pattern year after year and thus observations can be used to inform future trends and assist vessel navigation decision making. In this system, sixteen zones of increasing severity were identified within the Arctic region. Additionally, vessel ice classes were defined which included nine Arctic classes and five Baltic classes. Finally, opening and closing dates were determined for a given region and the types of vessel classes that could access a given region [61].

While a useful tool, it has long since been recognised that this method has serious limitations. First it does not account for long term trends and the change of ice conditions year after year [60] [62]. Firstly, it is a system that does not factor exceptions that can occur such as an unaccounted ship type or classes. Additionally, it does not consider changes in weather patterns where the expected ice conditions were different from the observed, which should be factored into decision making [60] [63]. This is further accentuated by the warming of the Arctic, which has meant that existing weather patterns have changed. These limitations motivated the search for other methods.

2.3.2. AIRSS Method

The Canadian Arctic Ice Regime Shipping System (AIRSS) is a system that was introduced in 1996 as a way to accommodate the observed or forecasted ice conditions [59] [62]. It introduced the concept of an ice regime, which is an area with a relatively similar distribution of different ice types, open water, and their associated partial concentrations [64], and is reported in ice charts using an Egg Code, as previously presented in Figure 2.1.

The AIRSS method involves the calculation of a risk value called the Ice Numeral which is calculated based on the defined ice regime and vessel ice class [62]. If the calculated Ice Numeral is greater than zero, then the vessel is allowed to enter the ice regime, otherwise the vessel is not allowed to enter the region [64]. This binary operating condition is a limitation of the method as it does not account for other factors that could reduce the risk of a vessel operating in the given region. This aspect was considered in the development of the POLARIS methodology, which is described in the following section.

2.3.3. POLARIS: Ship Decision Support Tool

In discussing the methods of tactical navigation support, it is useful to highlight one of the important tools used by vessel operators. This method, known as POLARIS, may be enhanced by some of the ideas highlighted in this present work.

2.3.3.1. Introduction to POLARIS

POLARIS, which is short for Polar Operational Limit Assessment Risk Indexing System, is a tool that is used in polar waters to compare a vessel's capabilities, per its specified ice class, with the existing ice conditions [16]. Its aim is to determine the most suitable vessel class that can undertake a voyage, as well as to help chart a safe path for navigation.

POLARIS was introduced through the International Maritime Organization's Polar Code [25]. The Polar Code establishes the regulatory requirements for, in part, the design, construction, and operation of vessels in Arctic and Antarctic regions. It sets standards by identifying risks and gives recommendations, including some that are mandatory, on how those risks can be mitigated [16]. One of the hazards identified in the Polar Code is the presence of sea ice. The Polar Code recommends shipowners and classification societies use decision support tools, such as POLARIS, in determining the requirements of vessel ice class [16].

POLARIS has five key components, and these are shown in Figure 2.4 and summarized as follows:

1. It is a combination of the International Association of Classification Society (IACS) Polar Class ice classes, as well as ice class equivalences with the other jurisdictions such as the Finnish Swedish Ice Class Rules. These help to define the ice capabilities of a given vessel.
2. It defines ice types consistent with the terminology used by the World Meteorological Organization (WMO) found on ice charts globally
3. POLARIS accounts for different ice regimes such as partial sea ice concentrations as well as zero ice concentrations.
4. In warm temperatures, POLARIS also accounts for the decay of ice.
5. POLARIS also considers that vessels operating with icebreaker support will be associated with different risk profiles as compared to the same type of vessels without icebreaker support.

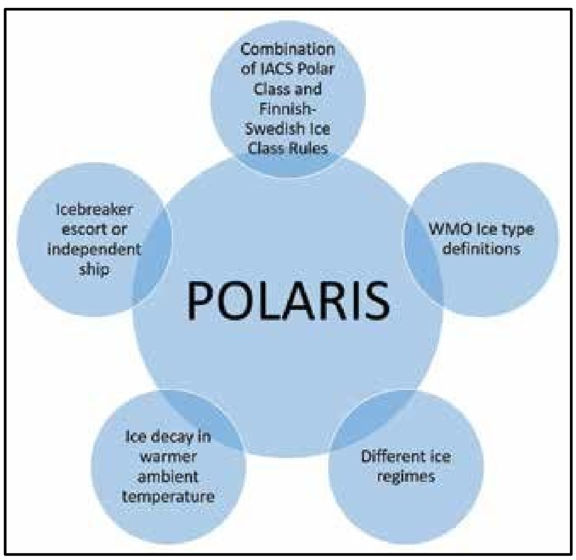

Figure 2.3 A summary of the five key elements of POLARIS [16]

In addition to the five key elements, POLARIS also utilizes Risk-Index Values (RIVs) to provide guidance on what vessels can do in certain situations [84, 85]. These are a key component of the decision support aspect of POLARIS. The RIVs indicate the risks associated with certain ice types and the risk assessment is completed by a Risk-Index Outcome (RIO) to define the operational limit of a given vessel. The results of these indices can permit or prohibit operation in a given ice regime. Additionally other adaptive measures can be recommended. These include limiting the vessel speed, increasing bridge watchkeeping or adding icebreaker support [84, 85].

Vessels operating in Arctic regions are assigned an ice class. This may be done following the International Association of Classification Societies (IACS) Polar Class system. The system identifies various categories ice class (referred to as Polar Class) based on the severity of ice conditions, and a ship is assigned a Polar Class based on their capabilities in ice [84, 85]. Table 2.2 below highlights the Polar Class classification system.

Table 2.1 showing the type of Ice that each ship Polar Class can navigate in [16].

Polar Class	**Ice Description (Based on WMO Sea Ice nomenclature)**
PC1	Year round operation in all Polar Waters
PC2	Year round operation in moderate multi year ice conditions
PC3	Year round operation in second year ice, which may include multi year ice inclusions
PC4	Year round operation in thick first year ice, which may include old ice inclusions
PC5	Yea round operation in medium first year ice which may include old ice inclusions
PC6	Summer/autumn operation in medium first year ice, which may include old ice inclusions
PC7	Summer/autumn operations in thin first year ice which may include old ice inclusions

Using the POLARIS system, there are guidelines that can be used as a reference when ship navigation is with elevated operational risk. These guidelines can be compared with the results obtained from the image processing. As a reminder, the POLARIS tool gives Risk Index Outcome (RIO) values for a given vessel type and ice conditions and then these RIO values are used to inform operations. Table 2.3 is an example of the RIO values as they relate to the vessel ice classes and the considerations for operations.

Table 2.2 showing the RIO values and their implications for various vessel ice classes [16]

RIO_{Ship}	Ice Classes PC1 – PC7	Ice Classes (Below PC7 and not assigned an ice class)
RIO > 0	Normal Operation	Normal Operation
-10 < RIO < 0	Elevated Operational Risk	Operation subject to special consideration
RIO <-10	Operation subject to special consideration	Operation subject to special consideration

Normal Operation means that the ice conditions encountered do not pose a threat to the vessel and thus a vessel can continue its normal operations without special consideration for the present ice regime.

Areas with elevated operational risk should be avoided for the purpose of voyage planning. If, during transit, it is necessary to enter a region of elevated operational risk, there are recommended speed limits based on ice class to reduce the operational risk. Speed limits are defined in Table 2.4. Generally, for RIO < -10, entry is prohibited.

Table 2.3 showing the POLARIS Ice Class classification and recommended speeds for elevated operational risk conditions [16]

Ice Class	Recommended Speed Limit
PC1	11 knots
PC2	8 knots
PC3-PC5	5 knots
Below PC5	3 knots

2.3.3.2. Limitations of POLARIS

POLARIS is not without its limitations. Firstly, POLARIS is not mandatory and is not explicitly mentioned in the Polar Code but regarded as a decision support tool that can be used to aid in navigation. Although it is implicitly recommended by the Polar Code, it is not mandated. This means it is not fully regulated and monitored, which presents the risk that it may not be necessarily fully enforced.

Secondly, POLARIS is partial in scope and is recommended not to be used as a final decision-making tool. This is because it only covers one aspect of a vessel's operating limitations i.e. the vessel performance in certain ice conditions. The Polar Code indicates that additional decision support tools are needed to assess whether a vessel can undertake a voyage [16]. Some of the aspects to consider include low air temperature; high latitude; the presence of icing on the vessel itself; as well as potential for collision with ice or land [16].

The third limitation is linked to how POLARIS does not account for the crew that may be operating the vessel. A crew's inexperience may affect how they operate in a particular environment. While certain requirements are indicated by the Polar Code for the training of the master and crew of a vessel, POLARIS does not account for the subjective nature of human operation, which is one of the major causes of accidents in ice environments [65] [66] [67]. Thus, despite the recommendations given by POLARIS, the final decision on the action taken is based on the qualified personnel onboard [16].

The major limitation of POLARIS in the context of this work and as a decision support tool is that while it accounts for the hull strength of a vessel in the determination of Polar Class or calculates a RIO value based on the ice conditions, it does not fully account for vessel particulars that will influence an operational area of relevance for a vessel. This is a significant limitation in terms of tactical navigation and this work seeks to highlight that limitation and show the other factors that should be considered.

In the context of the present work, the work discussed in this project is meant to demonstrate the potential benefit of camera sensors in supporting the efforts of the POLARIS system in aiding safe tactical navigation. Chapter 3 will focus on the methodologies employed to obtain the results presented later in this project.

2.4. Chapter Conclusion

In conclusion, this chapter provided an overview of the methods used for ice monitoring and their respective capabilities, emphasizing the importance of onboard cameras for this purpose. It also examined the guidelines and decision support tools available to assist ship personnel in making safe tactical navigation decisions. Specifically, the chapter highlighted the POLARIS recommended vessel speeds associated with different vessel ice performance ratings, which serve as the foundation for the analysis conducted in this study.

Chapter 3 Methodology

This chapter details the methodologies used to acquire image data and maneuverability parameters for evaluating the effectiveness of onboard cameras in tactical navigation support. It begins with the processing of camera data, where images are transformed to a top-down perspective, which is preferred for integration with maneuverability parameters. The chapter then outlines the methodology for calculating these parameters, ensuring that operational vessel characteristics are accurately reflected in the analysis.

The data sources for the image processing and calculations will be outlined in the final part of this chapter. Below is a summary of the methodology, in Figure 3.1, used for this research work and will be discussed in this chapter.

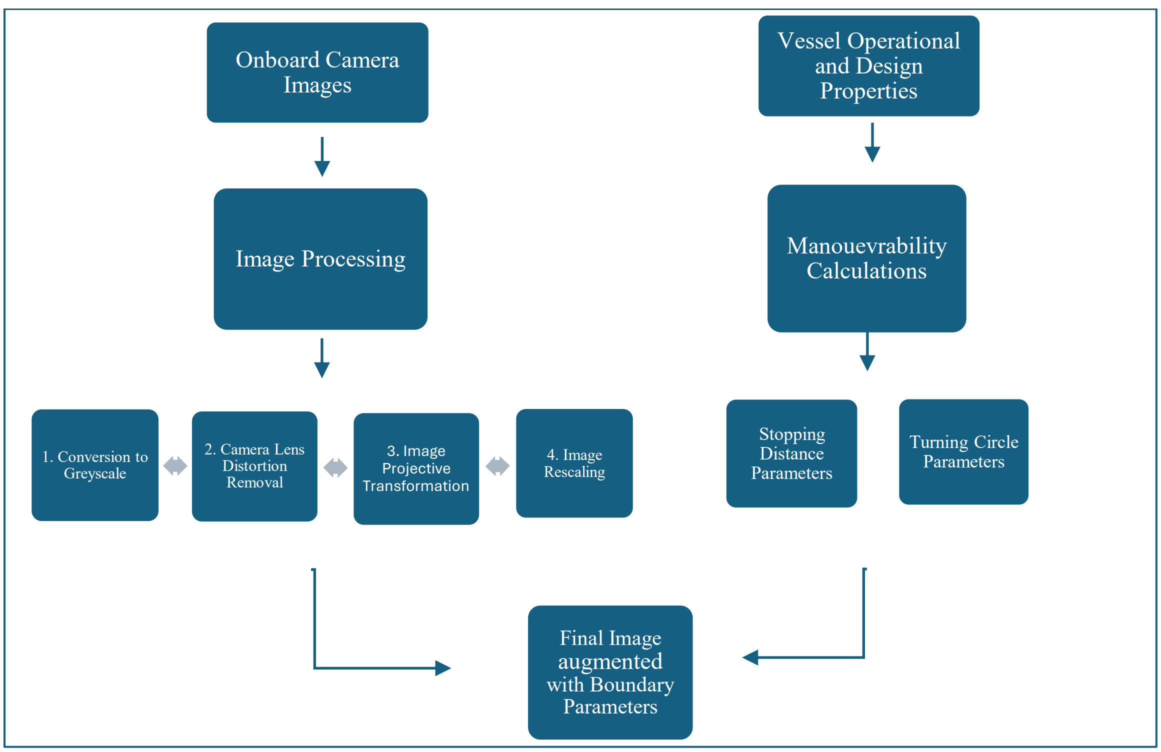

Figure 3.1 A high level summary of methodology outlined in Chapter 3

3.1. Image Processing

The transformation of the visual data is a muti-step process that will be outlined in this section. Figure 3.2 is a sample image from the footage recorded from the data collection campaign onboard the Amundsen icebreaker. This is the image that will be used as a sample for analysis throughout this work.

Figure 3.2 Forward view from the Amundsen vessel.

Figure 3.2 displays a forward view from the onboard camera. Transforming this view will involve several processing steps which include:

1. Converting to Greyscale and Contrast Enhancement
2. Camera Lens Distortion Removal
3. Camera Projective Transformation
4. Image Enlargement for True Scale.

The processing steps are described in the sections that follow.

3.1.1. Conversion to Greyscale and Contrast Enhancement

First the image is translated to a greyscale image so that it is in a format that can be used for further analysis, which involves the lens distortion removal and projective transformation. This would be extremely complicated and time-consuming to perform with a colour image with three values for a single pixel. In contrast, there is one value per pixel for greyscale images which depicts the pixel intensity. The conversion process is carried out using the MATLAB function *rgb2gray*.

After the greyscale conversion, the contrast of the image is improved using some inbuilt MATLAB functions. This helps to preserve the quality of the image as the preprocessing is carried out. There were several contrast improvement functions explored, and these included the following: *imadjust*, *histeq* and *adapthisteq*. These all give variable results. However, the selection of the function to use is one that gives the best contrast so that sea ice can easily be distinguished from the surrounding sea water. From observation, the *imadjust* function seemed to give the best contrast enhancement results.

3.1.2. Camera Lens Distortion Removal

The camera that was used to take the footage had some lens distortion. This can be observed in how the sea ice field image shown in Figure 3.2 depicts a curved horizon. Since the goal of this work is to compare the camera's field of view along with the vessel manoeuvrability parameters, the images used need to display a view of the ocean surface at true scale. This is done by using the camera intrinsic properties which are determined through a camera calibration process.

The determination of the camera intrinsic properties is carried out using the MATLAB function `estimateCameraParameters`. This function uses an input of images of a checkerboard of known dimensions in various positions of the image frame. Pictures of a checkerboard of known dimensions are taken at different positions in the camera view to accurately and fully account for the full lens distortion. This helps to determine the camera properties that will be used to rectify the image. Some of the images used are shown in Figure 3.3.

Figure 3.3 The checkerboard images that were used to determine the camera parameters

Support tasks were carried out to determine the input camera parameters utilized as inputs for this step. The MATLAB function `undistortImage` is used to apply these camera parameters.

The data was collected using a Sony HDR-AS100V action camera, as shown in Figure 3.4. The same camera model was used to capture calibration images required for lens distortion correction.

It is not certain whether the camera used for calibration was the exact same unit used for data collection, as multiple cameras of the same model were available onboard during data collection campaigns. This introduces a degree of uncertainty in the calibration results, as slight manufacturing variations between identical camera models can affect calibration accuracy. This limitation is acknowledged as a potential area for improvement in the calibration process. However, since the cameras were of the same model and type, the margin of error was considered minimal, allowing the image transformation process to proceed.

Figure 3.4 The Sony Action Camera used for the data collection.

After this calibration step, the camera properties are obtained and used to carry out the lens distortion removal process. The results from the process are shown in Chapter 4.

3.1.3. Camera Projective Transformation

Since onboard cameras are used in this project, one of the key areas to understand and explore is how to transform and manipulate the collected imagery data to obtain an image view that can be easily assessed and augmented with manoeuvrability parameter boundaries. This transformation involves the use of a principle called projective transformation, also known as homography.

Projective transformation is conducted by applying a matrix to the initial image so that it gives a transformed image. This matrix is known as the homography matrix [68]. The homography matrix is a transformation matrix that can be used to perform translation, rotation and warping transformations to other matrices [68] [69]. Since an image can be represented as a matrix with pixel values in its constituent locations, the homography matrix can be applied to it to achieve the desired transformation.

Since this principle is used to change the image views from one camera angle to another, it can be used to transform the image from the forward view to a top-down view for this project

[70]. This is more useful for augmenting with the vessel manoeuvrability parameters on the immediate sea ice field. An example of this transformation is provided in Figure 3.5.

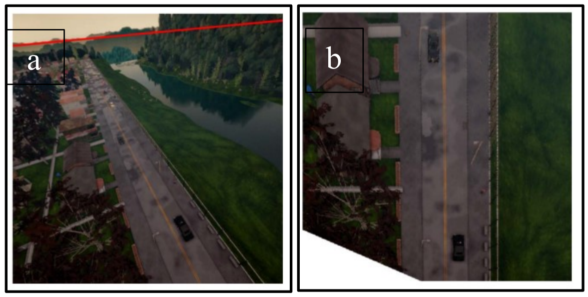

Figure 3.5 The sample transformation of a view from a forward-looking view (left) to a top-down view (right) [70]

In order to acquire the image that would give a top-down image view of the vessel surroundings, a homography matrix was applied to the image. The homography matrix transforms the angle of the camera view to achieve a different perspective, essentially obtaining the same picture from a different viewpoint. The homography matrix can be determined from the camera specifications as well as some details of how the camera was positioned during the data collection [71]. From first principles, the homography matrix can be determined by the following equation:

$$H = K * R * K^{-1} \qquad \textit{Equation 1}$$

where H is the homography matrix,

K is the camera intrinsic matrix and

R is the rotation matrix which represents image projective rotation.

The K matrix is the camera intrinsic matrix, and this is determined using the camera parameters [71]. These are obtained in the camera lens distortion removal process in Section 2.1.2. Below is the equation used to define the K matrix

$$K = \begin{pmatrix} \frac{fx}{Sx} & 0 & cx \\ 0 & \frac{fy}{Sy} & cy \\ 0 & 0 & 1 \end{pmatrix} \qquad \textit{Equation 2}$$

where *fx* is the focal length in the x direction,

Sx is the scaling factor length in the x direction,

fy is the focal length in the y direction while

Sy is the scaling factor in the y direction; and

cx and *cy* are the coordinates of the image's optical centre [71].

Similarly, the rotation matrix can also be defined. This helps to rotate the image from the forward view to the top-down view [Sandru et al].

$$R = \begin{pmatrix} 1 & 0 & 0 \\ 0 & cos\theta & -sin\theta \\ 0 & sin\theta & cos\theta \end{pmatrix} \qquad \textit{Equation 3}$$

where θ is the angle of the camera from the normal to the earth's surface (the angle between the two perspectives, initial and transformed) [71]

The angle is reflected in the image displaying the effect of the homography matrix labelled as H in Figure 3.6.

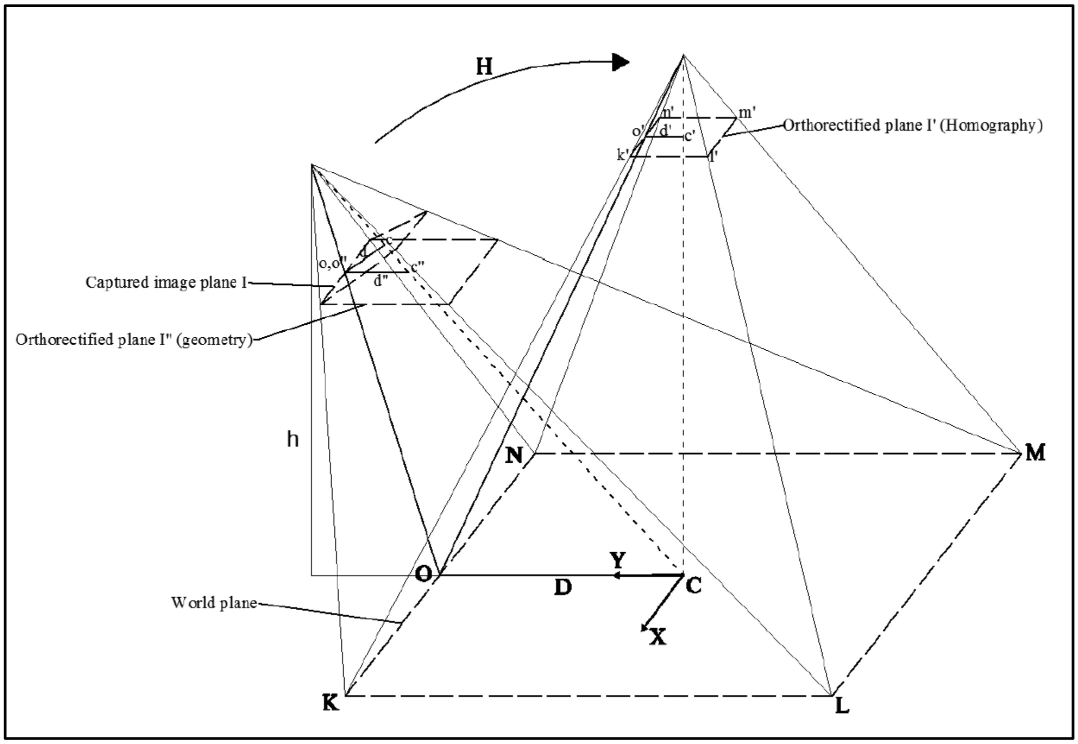

Figure 3.6 The desired transformation of the camera view to give a top view. [71]

Once the homography matrix has been determined, the matrix is applied to the source image to give a transformed image [68]. The homography matrix is a 3x3 matrix. The transformation is illustrated by the equation,

$$I' = H * I \qquad \text{Equation 4}$$

where I is the initial source image and

I' is the transformed image with the top-down view [68]

Homography principles are used to perform this transformation in MATLAB, using the functions `projective2d` and `imwarp`.

3.1.4. Image Enlargement for True Scale

In addition to the transformation to a top down view, the images also need to be scaled to reflect the true distance. This will help to ensure that the augmentation with the stopping distance and turning circle parameters will be accurate. This is carried out by applying varying scale factors to different pixels within an image. The principle used will be explained here. The challenge of true scaling in the image is depicted in Figure 3.7. As is expected in the image shown as Figure 3.7, the size of objects in a picture reduces in comparison to objects of the same size that are closer to the image source (camera). This is demonstrated by how the ice floes in the Figure 3.7 reduce in size as one moves away from the position of the camera. In other words, the pixel to distance ratio changes as one moves deeper into the image and away from the camera.

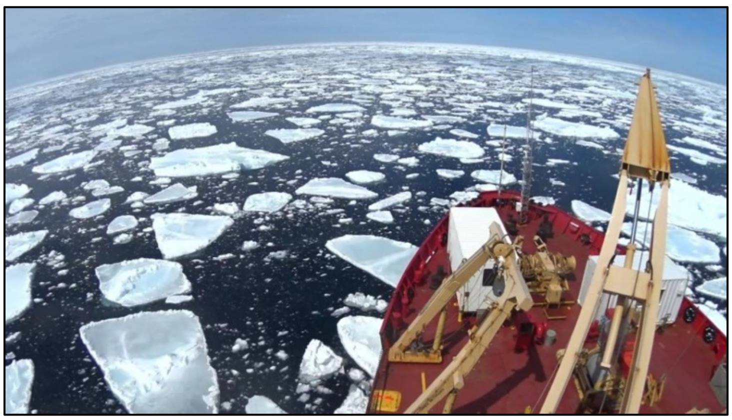

Figure 3.7 The forward view of the vessel

The pixel to distance ratio changes became the basis for the methodology used to enlarge the image. Essentially, a scale factor would be applied to each pixel in the image to enlarge it based on its distance from the camera.

This process makes use of the known distance to a reference feature on the image and the distance to the horizon, which can be calculated using a generic equation [81]. Finally, a correlation of the angle the camera makes with positions on the surface is related with the distance from the reference geometry to the horizon. Each increment in the angle is related to an increase in distance as one moves towards the horizon. A set of scale factors can be obtained which will then be used to enlarge the image to near true scale.

The process is outlined as a multi-step process as follows:

I. Scaling and Reference Geometry

II. Distance to Horizon Calculation

III. Determining Relevant Camera Angles

IV. Discretization of Pixels in Region of Interest

These are further elaborated in the following sections.

3.1.4.1. Scaling and Reference Geometry

Firstly, reference geometry of known dimensions is identified in the image, along with the distance to the horizon. In this case, since the data used in this research was acquired several years ago, measurements could not be done empirically. However, a feature of known geometry on the vessel itself was used. This is shown in Figure 3.9. Given that the image is drawn to scale and the full vessel length is information that is publicly accessible, the true size of the reference geometry could be attained by determining the scale in the image shown in Figure 3.8. The reference geometry is shown in the onboard image Figure 3.9.

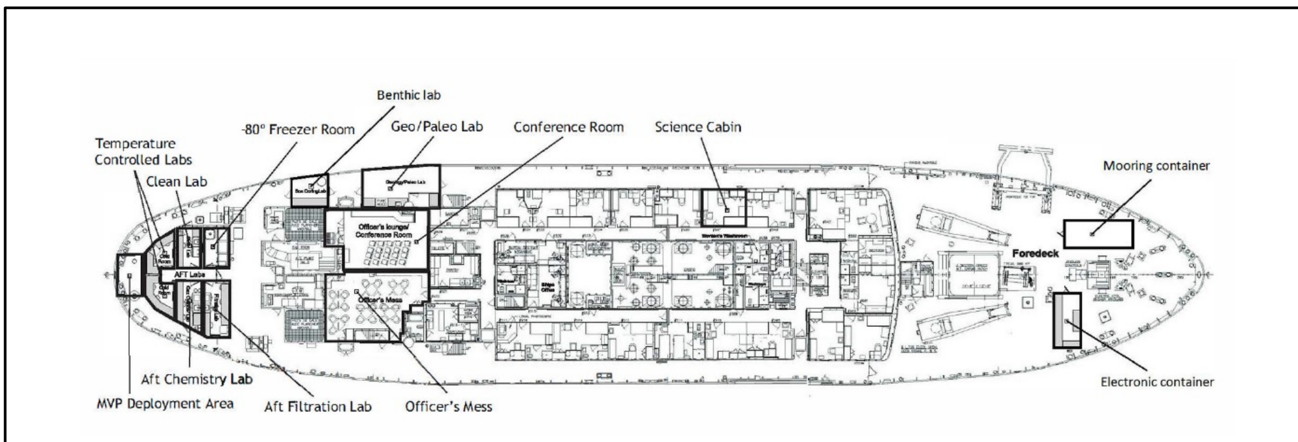

Figure 3.8 A scaled down schematic of the Amundsen vessel with the marked reference geometry (mooring container) [72]

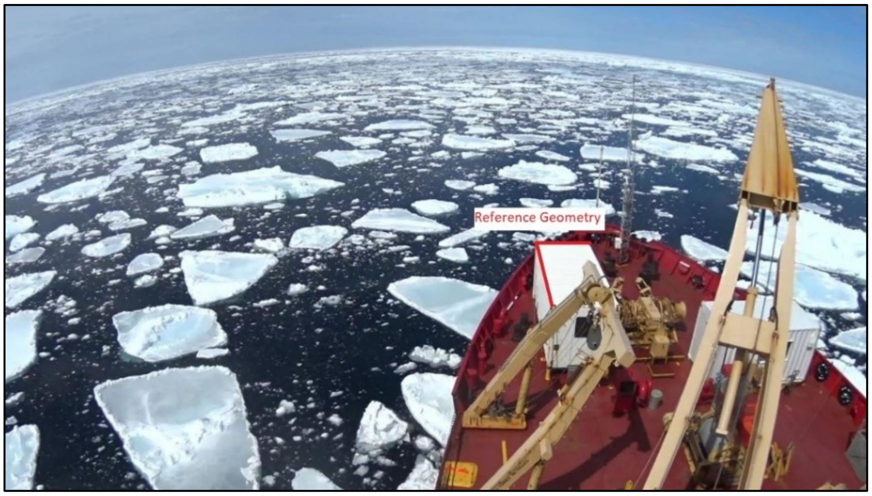

Figure 3.9 The labelled reference geometry for accurate scaling

3.1.4.2. Distance to Horizon Calculation

Additionally, the distance to the horizon was also determined using an arbitrary equation which is the following:

$$d = \sqrt{(12.756 * H)} \quad \text{Equation 5}$$

where *d* is the distance to the horizon in km and,

H is the height above sea level in m [73].

This simplified equation is derived from the following image in Figure 3.10:

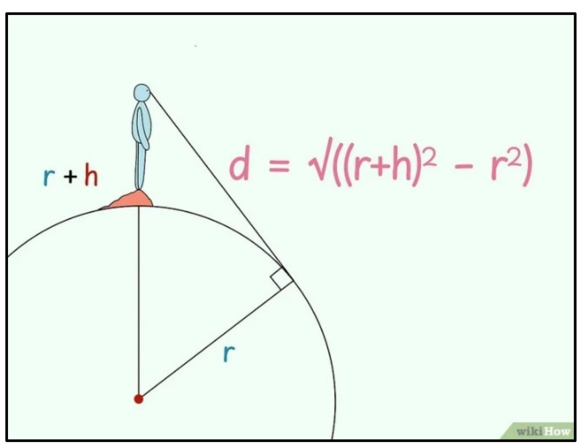

Figure 3.10 The derivation of the horizon distance calculation. [81]

The derivation can be derived using the Pythagoras theorem for the triangle shown in Figure 3.10 where,

$$a^2 + b^2 = c^2 \qquad \textit{Equation 6}$$

Using the figure shown above, let

a = *r* (radius of the earth)

b = *d* (distance to horizon) and

c = *(r+h)* (Earth's radius plus elevation).

This makes the above equation to the following

$$r^2 + d^2 = (r + h)^2$$

Rearranging to make the distance to the horizon the subject of the formula gives,

$$d = \sqrt{}((r + h)^2 - r^2)$$

$$d = \sqrt{}(2rh + h^2)$$

$$d = \sqrt{}(2r + h)h$$

Given that the value of the earth's radius (r = 6378km) will be significantly lower than that of the height above sea level (in this case around 0.02km for the camera height), the equation above can be simplified, with the value of the radius of the earth incorporated to give the following:

$$d = \sqrt{}(2rh) = \sqrt{}(2 * 6378\ km * h) = \sqrt{}(12\ 756 * h) = \sqrt{}(12.756 * H)$$

$$d = \sqrt{(12.756 * H)}$$

This gives the equation quoted at the beginning of this section where *d* is the distance in km and whereas the height *H* is in meters.

The horizon calculation assumes an orientation based on the angle between the camera and the farthest visible point on the horizon, as illustrated in Figure 3.10.

As demonstrated later in this research, the error in calculating the distance to the horizon is not significant, as ice features in the distant background are unlikely to be fully characterised due to the low resolution of far-field areas in the acquired images. The key focus is on regions within the vessel's operational area, defined by its turning radius and stopping distance.

The horizon is shown in Figure 3.11 and the magnitude of the distance from the camera to the horizon was noted for use in subsequent processing.

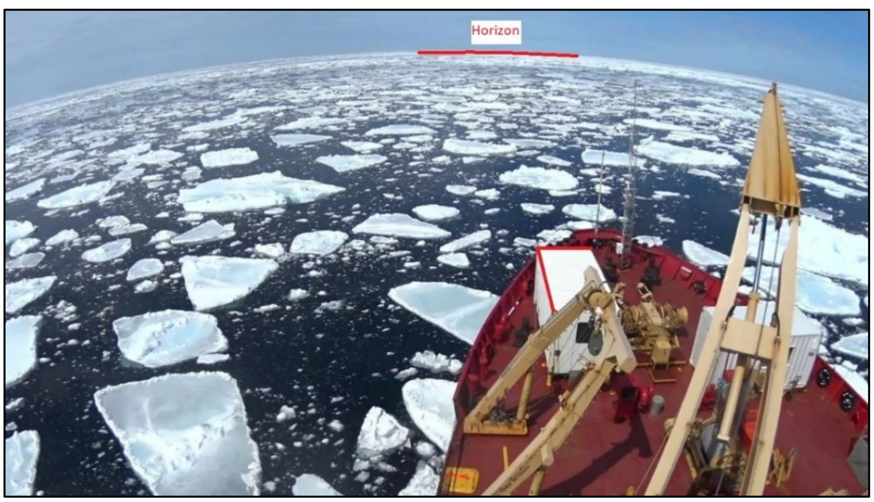

Figure 3.11 The horizon. Note that this is the raw data obtained from the onboard camera. Image processing will be carried out to remove distortion effects

3.1.4.3. Determining Relevant Camera Angles

A set of triangles are created to obtain the angles that the camera makes with the reference geometry and the horizon. These are demonstrated in the image below. These two angles are illustrated in Figures 3.12 and 3.13.

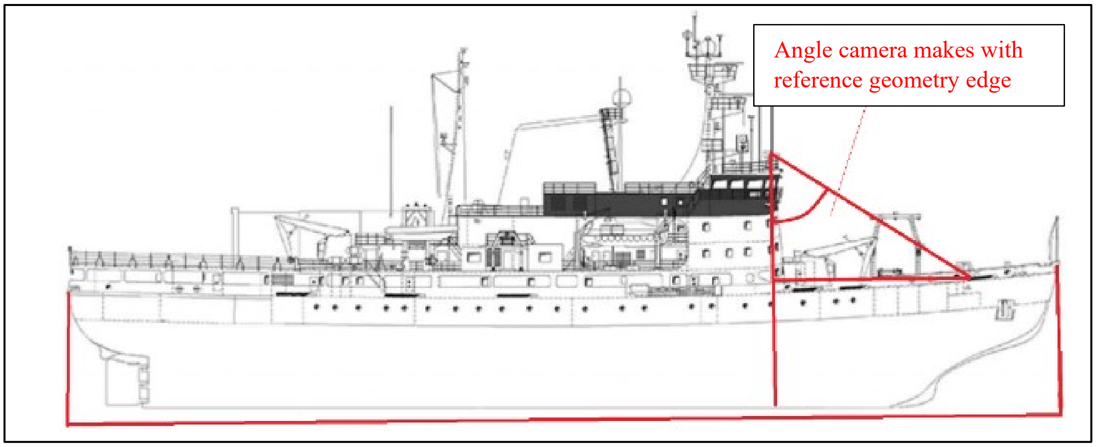

Figure 3.12 The angle the camera makes with the reference geometry edge [72].

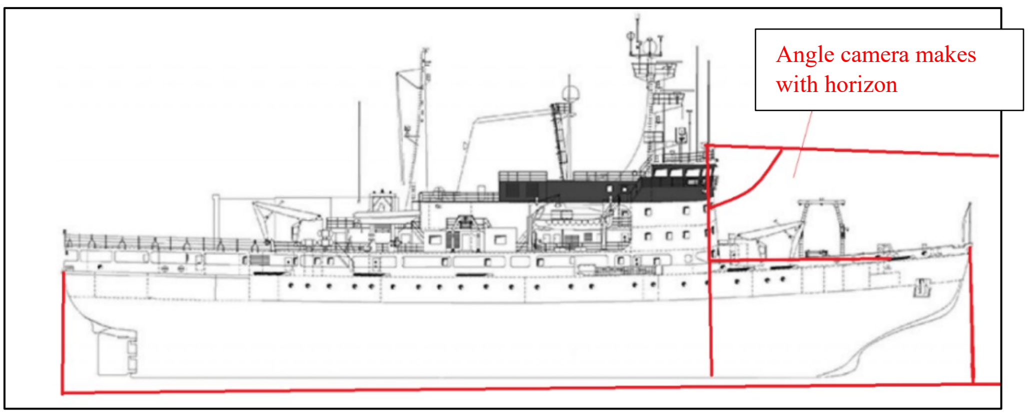

Figure 3.13 The angle the camera makes with the horizon

The distance between the edge of the reference geometry and the horizon is the region of interest and is the area that will be enlarged to show true scale. Figure 3.14 in the next step depicts this region of interest.

3.1.4.4. Discretization of Pixels in Region of Interest

Once the range of the angle is determined, along with the distances of the reference edge and horizons from the camera, discretization of the image can be performed to determine the angle increment. This consequently provides the distance increment for each pixel increment from the reference geometry to the horizon in the region of interest. This region is shown in Figure 3.14.

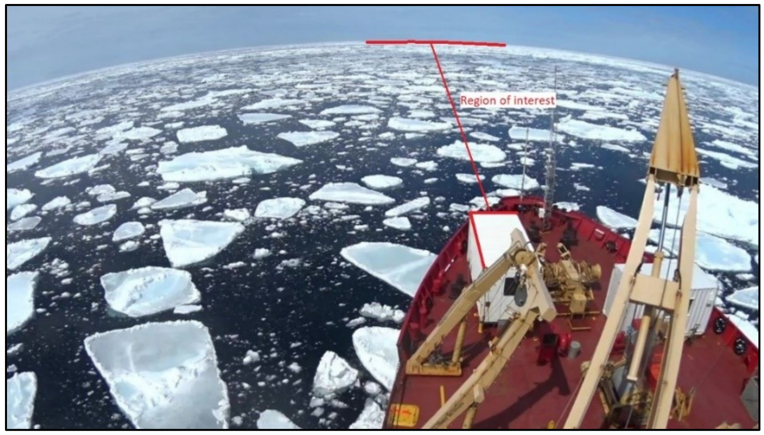

Figure 3.14 The region of interest. Once transformed, this region of interest will be used for the discretization of pixels

The outcome from the processing step above will be an image that has been enlarged using the relationship between each pixel and its associated distance increment. The results are shown in Chapter 4.

3.2. Vessel Manoeuvrability Parameters

To demonstrate the effectiveness of onboard cameras, imagery will be compared to the vessel's manoeuvrability capabilities, particularly from a hazard avoidance perspective. This section discusses the parameters that will be used to define the vessel's manoeuvrability. These parameters are defined by the International Maritime Organization (IMO) in the American Bureau of Shipping (ABS) Manoeuvrability Guide and include the vessel's stopping distance, advance and transfer parameters [74]. These parameters are further defined in the sections that follow.

The manoeuvrability parameters will be determined using the stopping distance and turning circle tests. Table 3.1 gives the definitions of the parameters.

Table 3.1 showing a summary of the manoeuvrability parameters used for this work

Test	Parameters	Definitions
Stopping Distance	Stopping Distance	Distance along the initial trajectory before stop
Turning Circle	Advance	Distance along the initial trajectory before turn
	Transfer	Distance travelled normal to initial trajectory

3.2.1. Stopping Distance Test

There were two methods that could have been used to calculate the stopping distance parameter. The first method, which does not fully account for the vessel operational parameters, is based on vessel type [74]. In contrast, the second method accounts for the vessel operational parameters in its equations. Figure 3.15 shows us the stopping distance test and the parameters associated with it.

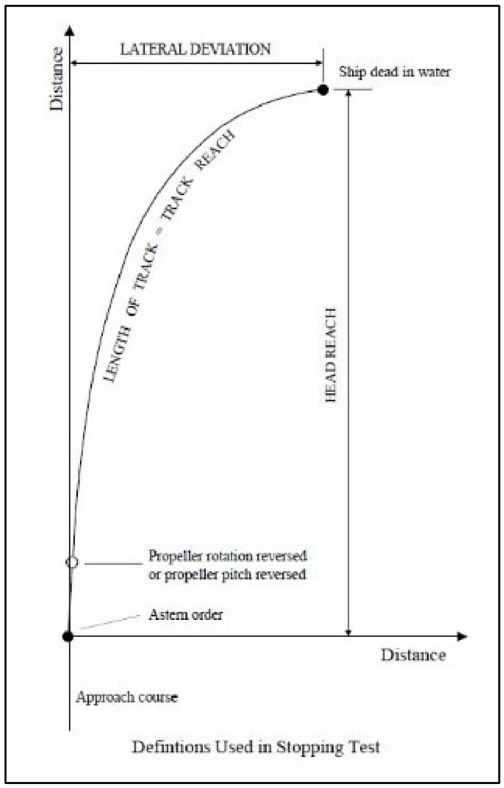

Figure 3.15 The stopping distance test. The stopping distance is called termed head reach in this test [74]

3.2.1.1. Method 1

As indicated earlier in this section, there are two ways to determine the stopping distance. One method is to determine the stopping distance based on vessel type, while a second method uses equations to account for vessel operational conditions. To calculate the stopping distance using the vessel type, the following equation is used:

$$S = Alog(1 + B) + C \qquad \text{Equation 7}$$

where S is the stopping distance in ship lengths

A is a dimensionless parameter linked to the type of vessel and

B is a dimensionless vessel linked to the type of vessel engine and

C is a parameter associated with vessel speed and time to reverse thrust [74]

These dimensionless parameters *A, B* and *C* are then defined for the different options in the ABS guide. For the determination of A, the guide provides two values for each case, a lower bound and an upper bound. The value of A is shown to be dependent on the vessel type. These are shown in Table 3.2.

Table 3.2 shows the values for the co-efficient of A for different vessel types [74]

Vessel Type	**Coefficient A**	
	Low Boundary A_{low}	**High Boundary A_{high}**
Cargo Ship	5	8
Passenger Ferry	8	9
Gas Carrier	10	11
Product Tanker	12	13
VLCC* * *Very Large Crude Carrier*	14	16

As can be seen, the values in the table for the parameter A are limited to only five types of vessels which limits the applicability of this method to other vessel types such as an icebreaker. This is one of the motivations for the use of the second stopping distance calculation method, which will be shown in the next section. The second parameter B can also be illustrated as shown in Table 3.3.

Table 3.3 showing the parameters for Coefficient B [74]

Type of Machinery	Coefficient B	
	Low Boundary B_{low}	**High Boundary B_{high}**
Diesel	0.6	1.0
Steam Turbine	1.0	1.5

As shown in Table 3.3, there are only two types of engines accounted for in this method. Method 2 will seek to calculate the resistance and the thrust for each vessel to calculate the stopping distance without being limited by generic values for only two vessel engine types.

Finally, the *C* parameter from Equation 7 is determined based on the time it would take for each vessel to achieve reverse thrust as well as the initial vessel speed. This is shown in the equations below.

$$C = \begin{cases} C_L & if\ Vs < 15kn\ \ or\ T_{Rv} < 60 \\ C_L \frac{V_S}{15} & if\ Vs > 0.25T_{Rv} \\ C_L \frac{T_{Rv}}{60} & if\ Vs \le 0.25T_{Rv} \end{cases} \qquad \text{Equation 8}$$

Where V_s is the vessel speed in knots,

T_{Rv} is the time to achieve reverse thrust in seconds, and

C_L is a coefficient that depends on length.

The C_L coefficient can be calculated as follows:

$$C_L = \begin{cases} 2.3 & if\ L \le 100m \\ -0.012 * L + 3.5 & if\ 100m < L \le 200m \\ -0.003 * L + 1.7 & if\ 200m < L \le 300m \\ 0.8 & if\ L > 300m \end{cases} \qquad \text{Equation 9}$$

where *L* is the length of the vessel.

Therefore, with all the constituent terms calculated, the stopping distance values can then be determined using Equation 7.

3.2.1.2. Method 2

The second method builds on the theory used in the first method and seeks to refine the equations so that they can be used for a wider application of vessel types [Sung et al]. As illustrated in the previous section, the types of vessels that can be used for the Method 1 equations are only limited to the five types. Additionally, it is also desirable to effectively account for the effect of the vessel operational parameters as this will affect the stopping ability of a vessel. The second method makes use of the following equation.

$$S = \frac{(m + m_x) \cdot V_0^2}{2R_0} \cdot ln\left(1 + \frac{R_0}{T_S}\right) + \frac{V_0 \cdot t_r}{2} \qquad \textit{Equation 10}$$

where *S* is the stopping distance in m

m is the mass of the vessel,

m_x is the surge added mass (normally assumed to be 8% of vessel mass, [Sung et al])

V_0 is the approach speed of the vessel,

R_0 is the resistance of the vessel prior to the stopping maneuver,

T_S is the full astern thrust of the vessel, and

t_r is the time taken to reverse the shaft [75].

This equation is similar to Method 1 for stopping distance and this can be shown by equating the terms in the equation with the three coefficients from Method 1. These are the following:

$$A = \frac{(m + m_x) \cdot V_0^2}{2R_0} \qquad \text{Equation 11}$$

$$B = \frac{R_0}{T_S} \qquad \text{Equation 12}$$

$$C = \frac{V_0 \cdot t_r}{2} \qquad \text{Equation 13}$$

It is worth noting that there are other ways that stopping distances are determined and these include the use of braking indices derived from full-scale trials or simulations [76]. Computational Fluid Dynamics (CFD) and manoeuvring simulation software enable detailed analysis of hydrodynamic effects on ship motion which account for hull shape, propulsion system efficiency, and environmental conditions in determining stopping distance [77]. In addition to these, there are also vessel bridge systems fitted with radar and GPS to detect the vessel's position and speed and consequently provide an estimate of stopping distance [78]

However, since the IMO standard is a regulatory guideline, these parameters were used as conservative estimates. Additionally, the stopping distances calculated does not account for ice drag effects since the stopping distance test as defined by the IMO is for open water. This also adds to the conservative nature of the stopping distance calculated in this work.

Incorporating the effect of ice drag on the vessel is expected to reduce stopping distances due to the additional drag force. However, since regulatory stopping distance calculation standards do not account for ice drag, it is not addressed in this study. Future research could explore this aspect by incorporating an ice drag term into stopping distance calculations to more accurately reflect variations based on ice concentration [82]. Figure 3.16 below shows the effect of the ice concentration on the resistance terms for vessels.

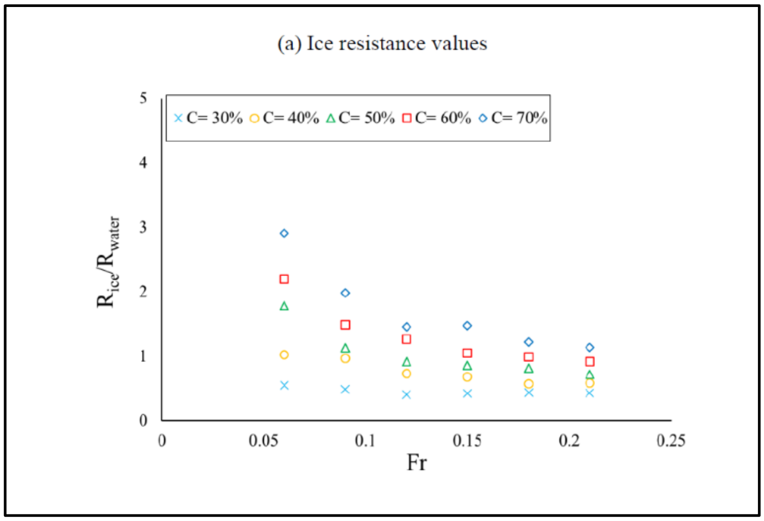

Figure 3.16 The effect of ice concentrations on the resistance faced by the vessel [83]

In summary, the effect of ice is not included in the calculations in this study, as significant ice concentrations are required to notably impact stopping distance and turning radius, as shown in Figure 3.16. Since the POLARIS framework ensures that vessels do not operate in heavy ice conditions without icebreaker support, the impact of higher ice concentrations is beyond the scope of this research but could be explored in future studies

3.2.2. Turning Circle Test

The turning circle test has two parameters that define the extent of a vessel's manoeuvrability for a 90-degree turn. These two are the vessel Advance and Transfer as illustrated in Figure 3.17. The figure also depicts the intermediate parameters that are obtained in the calculations of the Advance and Transfer.

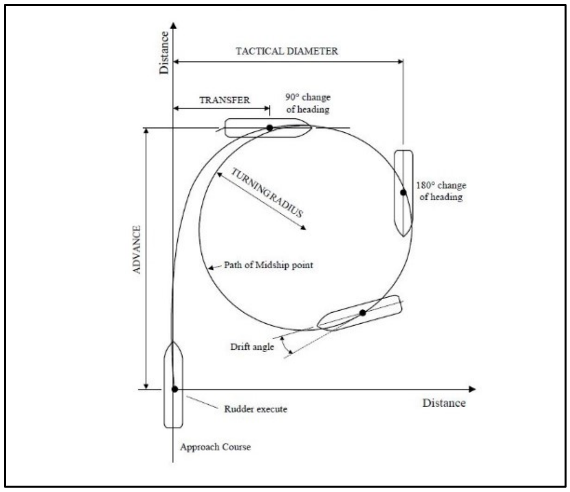

Figure 3.17 The turning circle test used to determine the advance and transfer parameters [74]

The two parameters to be determined for the turning circle are the transfer and advance parameters. These are determined by obtaining constituent parameters and then using them in the final equations. First a parameter known as the Steady Turning Diameter (STD) is defined, this will be used in further equations to determine values of interest.

$$\frac{STD}{L} = 4.19 - 203\frac{C_B}{\delta_R} + 47.4\frac{Trim}{L} - \frac{13.0B}{L} + \frac{194}{\delta_R} - 35.8\ \frac{SP*Ch}{L*T}(ST-1) +$$
$$+3.82\frac{SP*Ch}{L*T}.(ST-2) + 7.79\frac{A_B}{L*T} + 0.7\left(\frac{T}{T_L}-1\right)\left(\frac{\delta_R}{|\delta_R|}\right)(ST-1) \qquad \textit{Equation 14}$$

Where *STD* is the steady turning diameter,

C_B is the block coefficient,

δ_R is the rudder angle in degrees,

Trim is the vessel static trim,

L is the length of the vessel,

B is the modeled breadth of the vessel,

S_p is the span of the rudder,

Ch is the mean chord of the rudder,

T is the design draft at full load,

ST is the stern type,

T_L is the draft at which turning circle is estimated; and

A_B is the submerged bow profile area [74].

As can be seen, there are many inputs required for the calculation of the Steady Turning Diameter. Some of the terms are not available for the vessels and thus generic values from a sample vessel were used. Once the Steady Turning Diameter has been determined, the tactical diameter can then be calculated, which will then be used to determine the Advance and the Transfer values.

$$\frac{TD}{L} = 0.910\,\frac{STD}{L} + 0.424\,\frac{V_S}{\sqrt{L}} + 0.675 \qquad \textit{Equation 15}$$

$$\frac{Ad}{L} = 0.519\frac{TD}{L} + 1.33 \qquad \textit{Equation 16}$$

$$\frac{Tr}{L} = 0.497\frac{TD}{L} - 0.065 \qquad \textit{Equation 17}$$

Where *TD* is the Tactical Diameter in m,

L is the length in m,

STD is the steady turning diameter in m,

Vs is the test speed in knots,

Ad is the Advance in m and

Tr is the Transfer in m [74].

These parameters are then used to assess the manoeuvrability and consequently, the ability of a vessel to change direction should it encounter an ice hazard.

Additionally, the extra ice drag is expected to influence the vessel's turning radius by increasing resistance to its turning force. This could result in a larger turning radius, though the extent of this effect depends on ice concentration [82, 83]. Further research could examine the impact of ice resistance on vessel maneuverability. Figure 3.18 below illustrates this effect for an ice concentration of approximately 70%.

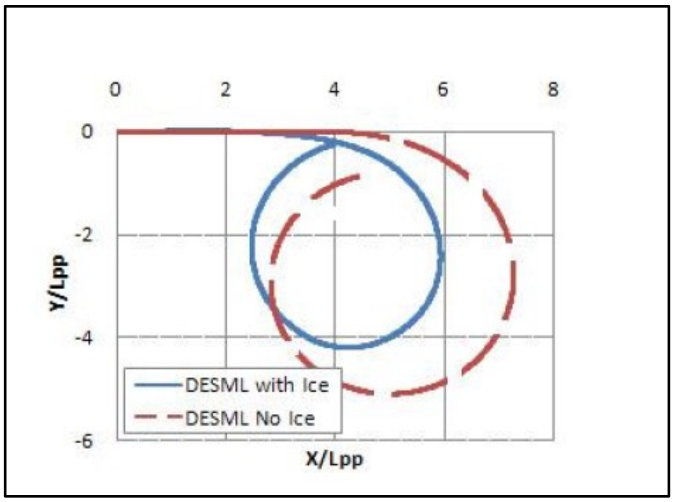

Figure 3.18 The two results for the same vessel in ice and without ice for simulation for turning circle. [82]

In summary, the effect of ice is not included in the calculations in this study, as significant ice concentrations are required to notably impact stopping distance and turning radius, as shown in Figure 3.18. Since the POLARIS framework ensures that vessels do not operate in heavy ice conditions without icebreaker support, the impact of higher ice concentrations is beyond the scope of this research but could be explored in future studies.

3.2.3. Effect of Vessel Properties on Stopping Distance and Turning Circle

One of the important factors to consider is that certain vessel parameters affect the manoeuvrability parameters. The equation for the stopping distance is shown to be the following:

$$S = \frac{(m + m_x) \cdot V_0^2}{2R_0} \cdot ln\left(1 + \frac{R_0}{T_S}\right) + \frac{V_0 \cdot t_r}{2} \qquad \textit{Equation 18}$$

In addition, there is also the turning circle parameters which are the Advance and Transfer. The equations for these are shown below.

$$\frac{Ad}{L} = 0.519\frac{TD}{L} + 1.33 \qquad \textit{Equation 19}$$

$$\frac{Tr}{L} = 0.497\frac{TD}{L} - 0.065 \qquad \textit{Equation 20}$$

To illustrate the effect of vessel particulars on these manoeuvrability parameters, certain vessel properties were used for calculations. These vessel properties are highlighted in Table 3.4.

Table 3.4 showing the properties of three sample vessels [72] [74].

Example Vessel	Length L (m)	Breadth B (m)	Draft (m)	Mass (metric tons)
Sample 1	98	19.5	7.2	5911
Sample 2	189	26.6	11.7	22 462
Sample 3	350	58.3	19.4	355 600

To illustrate the effect of key vessel particulars, the graphs of the stopping distance compared to speed are illustrated below, first showing the stopping distance in ship lengths in Figure 3.19 and then finally in meters in Figure 3.20.

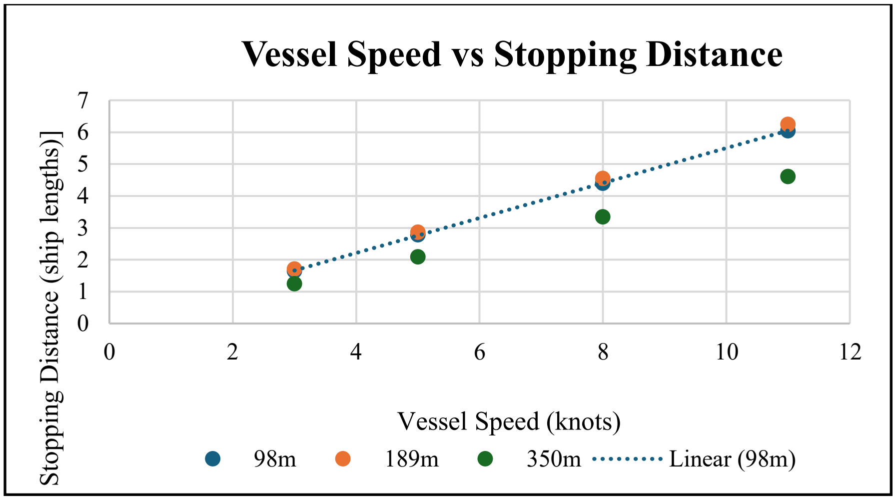

Figure 3.19 Vessel Speed vs Stopping Distance in ship lengths

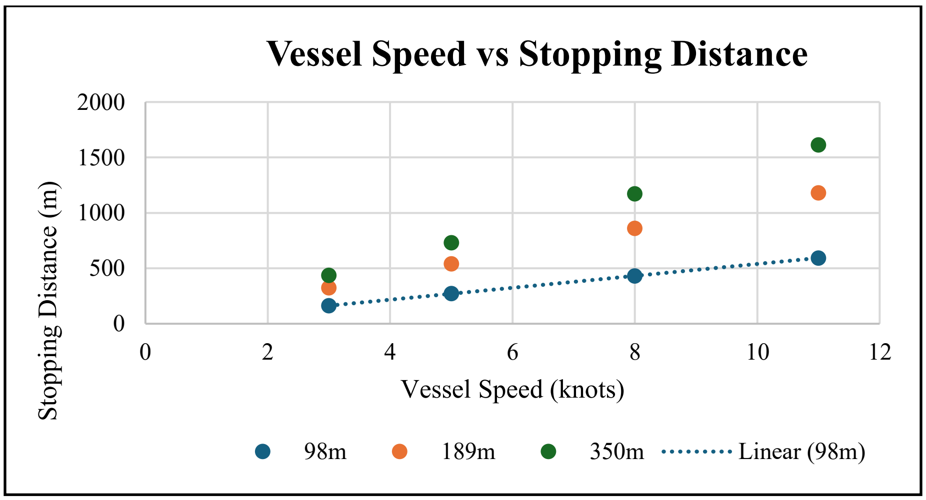

Figure 3.20 Vessel Speed vs Stopping Distance in meters

As can be seen from the stopping distance graphs, there is a linear relationship between the vessel speed and the stopping distance for all three sample vessels, indicating that the stopping distance is heavily influenced by the vessel speed. Additionally, it is also evident that typically, the higher the vessel length, the higher the vessel stopping distance.

For the turning circle parameters of Advance and Transfer, a similar illustration can be shown to highlight the effect, if any, that the vessel speed and the vessel length will have on the parameters. The results are shown in the Figures 3.21 and 3.22.

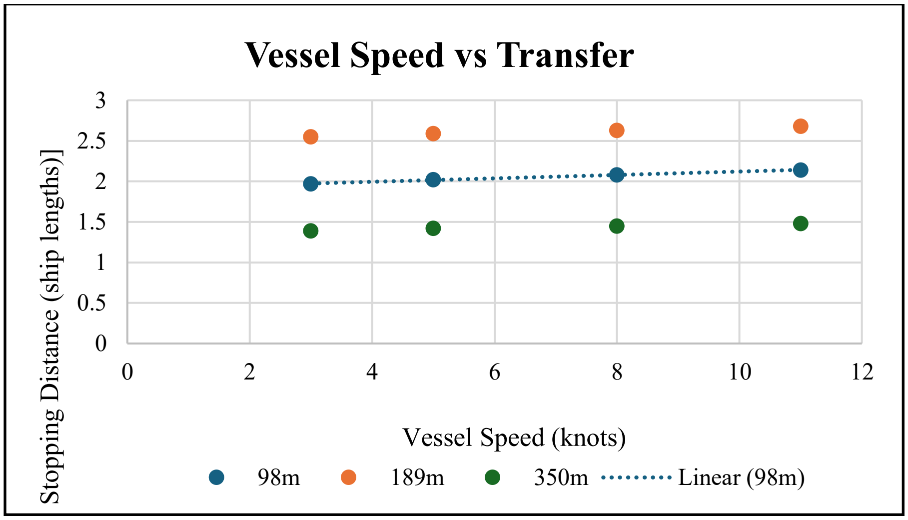

Figure 3.21 Vessel Speed vs Transfer in ship lengths

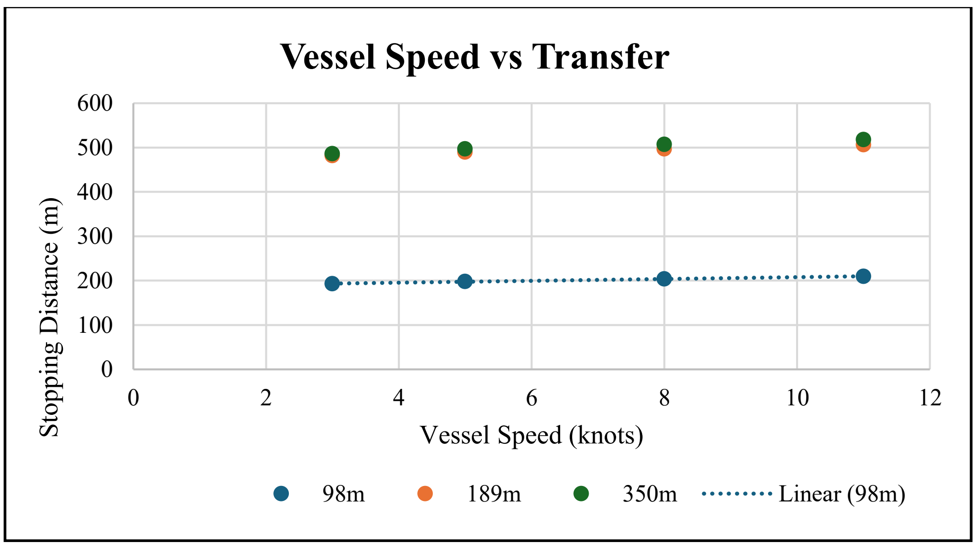

Figure 3.22 Vessel Speed vs Transfer in meters

Similarly, the relationship between the Advance parameter can also be shown to illustrate the effect of vessel speed and vessel length. These are shown in ship lengths in Figure 3.23 and in meters in Figure 3.24.

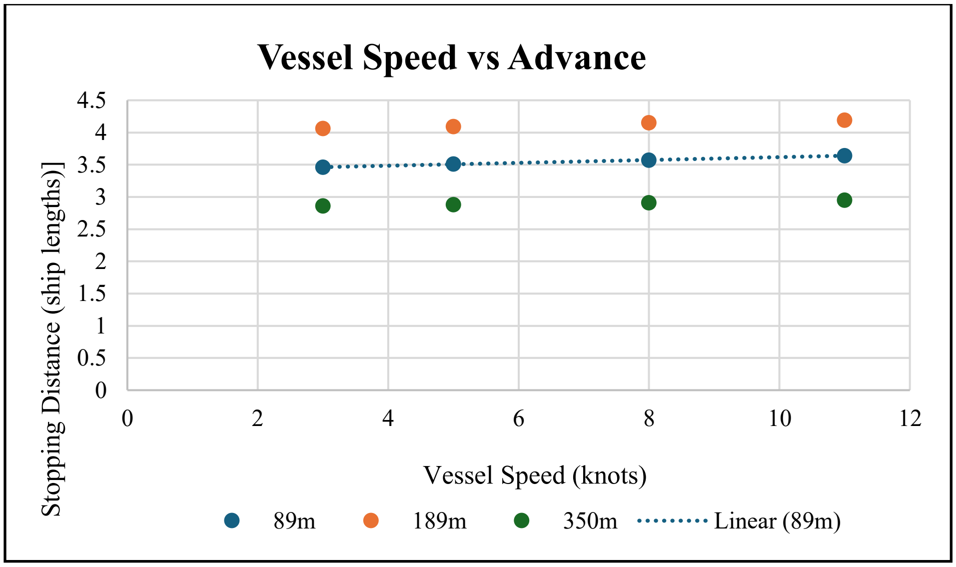

Figure 3.23 Vessel Speed vs Advance in ship lengths

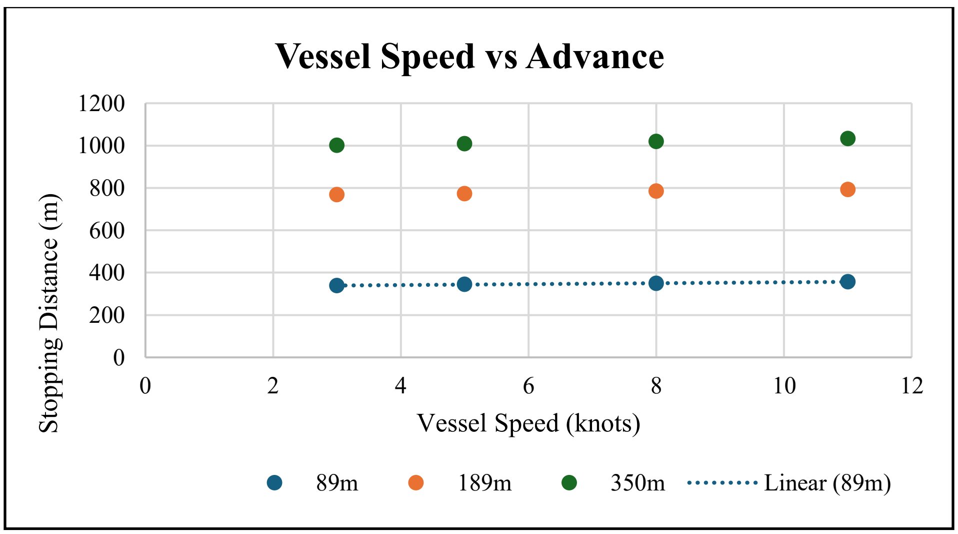

Figure 3.24 Vessel Speed vs Advance in meters

As is shown for both the Advance and Transfer parameters, the variation in speed for a given vessel does not seem to have a drastic impact on the Turning Circle, highlighting that other factors are more influential. For instance, it can be seen that the general trend in Figure 3.23 shows that as the vessel length increases, the turning circle parameters also tend to increase as shown in both the Advance and Transfer graphs.

Once the Stopping Distance and Turning Circle parameters are determined, the next step would be to augment the parameters with the visual imagery obtained from the onboard cameras. This augmentation will help to assess the effectiveness of the onboard cameras from an operational perspective. This step was described earlier in this chapter under the Image Processing section.

3.3. Data Sources

In addition to the methodologies employed in this work, a note is also made on the data sources used for the images and vessels analyzed.

3.3.1. Image Data Sources

In this work, the main data source for the images was the footage from an expedition by a Canadian Coast Guard Ship (CCGS) called the Amundsen. This footage had several view perspectives which included

i.) Forward Aft view

ii.) Backward Stern view and a

iii.) Port side left view.

All these views provided a unique perspective for the viewing of the different ice views of the ice regime surrounding the vessel. The footage was taken from an expedition that took place between 23 to 27 April 2015.

Additionally, the expedition spanned multiple days across different locations and different times, providing a sample that could be used to assess performance of any analysis in different settings. There were also instances of different visibilities, such as foggy, rainy, dark, overcast and sunny conditions. The data set included over 40 hours of footage. In this present work, the focus was on showing a forward view in clear conditions to demonstrate the capabilities of camera systems for tactical navigational support for vessels.

3.3.2. Vessel Properties

Publicly available resources and vessel specification documents were used to determine particulars for different vessels. The idea was to provide a sample of data for the different vessel classes that would need ice monitoring support.

In addition to the vessel particulars for the sample vessels presented previously in Table 3.4, which were used for the calculation of stopping distance and turning circle, there were other parameters used for the thrust calculations which are shown in the Table 3.5. The table displays a condition known as Maximum Continuous Rating (MCR). This is the condition where the vessel is considered to be operating at 85% of its full engine capacity and is used to demonstrate a vessel's capabilities [75]. Additionally, the vessel type is also used in some calculations and is noted for the sample vessels.

Table 3.5 showing the vessel particulars related to the vessel engine performance [74] [75}

Type of vessel	Example Vessel	MCR Speed (knots)	MCR Vessel (BHP)	Draft (m)	Propeller (RPM)
Icebreaker	Sample 1	16	13 600	7.2	85
Bulk Carrier	Sample 2	13.5	29 171	11.7	85
VLCC	Sample 3	16	30 000	19.4	83

Table 3.6 below gives more parameters of the vessels used for the Stopping Distance and Turning Circle calculations.

Table 3.6 showing further details about each vessel type and engine type [74]

Type of vessel	Example Vessel	Length L (m)	Vessel type Used	Engine Type Used
Icebreaker	Sample 1	89	Cargo Ship	Diesel
Bulk Carrier	Sample 2	189	Cargo Ship	Diesel
VLCC	Sample 3	350	VLCC	Diesel

It is necessary to estimate the block coefficient of the sample vessels. Generic ranges for the block coefficient for different vessel types are provided by *A. Charchalis et al 2013* and presented in Table 3.7. The block coefficient may also be calculated based on vessel particulars, as per Equation 21, and which are summarized for the sample vessels in Table 3.8.

Table 3.7 showing sample block co-efficient ranges for each vessel type [79] [80]

Vessel Type	Block Coefficient Range
Tanker	0.8 – 0.85
Bulk Carriers	0.82
Container Ships	0.60 – 0.76
Icebreaker	0.58-0.60

$$C_B = \nabla / LBT. \qquad \textit{Equation 21}$$

Where ∇ *is the volume displacement of the vessel,*

L is the length of the vessel

B is the vessel breadth, and

T is the vessel draft

Table 3.8 showing the block coefficient based on calculations from first principles

Type of vessel	Example Vessel	Length L (m)	Block Coefficient
Icebreaker	Sample 1	89	0.42
Bulk Carrier	Sample 2	189	0.37
VLCC	Sample 3	350	0.88

3.3.3. Speeds for Calculating Manoeuvrability Properties

The speeds used for the calculations for the manoeuvrability parameters were determined from the recommended speeds for Polar Class vessels operating under elevated risk conditions. These were obtained from Table 2.4 in Chapter 2.

3.3.4. Time Taken to Achieve Reverse Thrust Parameter

A parameter that was needed for the calculation of the stopping distance was the time taken to achieve reverse thrust. Since this information was not readily available, the data from sea trials of similar vessel types are used. These are shown in Figure 3.25 of the Coasting Time graph and subsequently documented in Table 3.9.

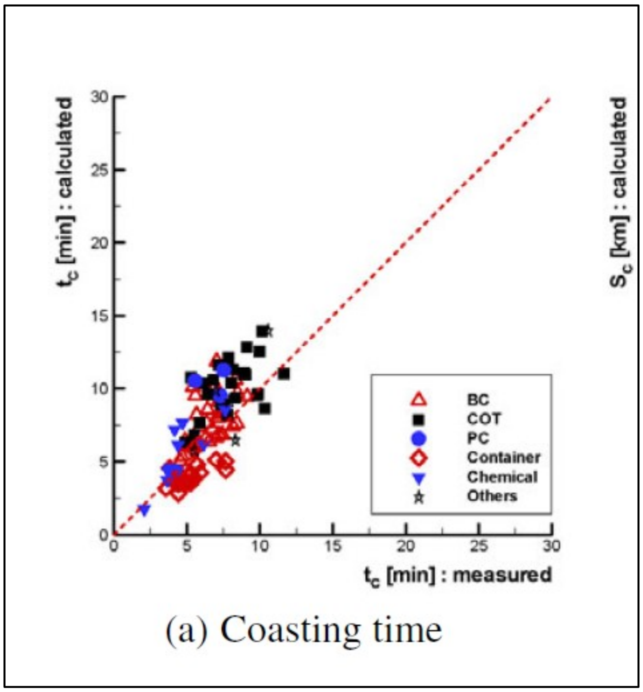

Figure 3.25 The values of the parameter of Time to Achieve Reverse thrust [75]

Table 3.9 showing the coasting values for typical vessels

Vessel type	**Coasting Time**
Bulk Carrier	7
Container	7.5
Cargo Oil Tanker	8.5
PC	7.5
Chemical	5
Others	7.5

3.3.5. Other Parameters

The other parameters that were required as input are generally not available as publicly available data. Coasting speed, Reynolds Number, and volume displacement were calculated as per Table 3.10. The values for thrust ratio, open water efficiency, relative rotation efficiency, and propeller RPM are defined as constants based on the values used in the ABS Manoeuvrability Guide [74], which are also presented in Table 3.10.

Table 3.10 showing the assigned values and equations used to obtain some of the inputs

Parameters	**Value or Equation**
Coasting Speed	Vessel Recommended Speed
Reynolds Number	Length*Vessel Speed/ Kinematic Viscosity
Volume Displacement	Displacement*Water Density
Thrust Ratio	0.55*
Open Water Efficiency	1.0*
Relative Rotation Efficiency	0.65*
Propeller RPM	85*

**values from [74] [75].*

3.4. Chapter Conclusion

This chapter outlines the methodologies employed for the key image transformation processes, including an introduction and explanation of projective transformation. Additionally, the equations used to calculate the manoeuvrability parameters for analysis are provided, along with an explanation of the relationship between these parameters and vessel properties. It is observed that initial vessel speed has a linear relationship with stopping distance, while the turning circle is primarily influenced by vessel length, with vessel speed having minimal impact. Finally, the data sources for the calculations to be carried out are presented, including from sample vessels.

Chapter 4 Results

The results from the methodologies and calculations that were described in Chapter 3 are presented in this chapter. These include the results from the image processing steps, the transformations and the manoeuvrability parameter calculations. Additionally, the augmentation of the transformed images with the manoeuvrability values is presented.

4.1. Image Processing and Transformations

The image processing steps included the conversion to greyscale, camera lens distortion removal, homography transformations as well as image enlargement. The results from these steps are shown in this chapter, along with descriptions of the results

4.1.1. Conversion to Greyscale and Contrast Enhancement

The sample image used for the processing steps is shown in Figure 4.1. It is in color and the first processing step involved changing it to greyscale using the MATLAB function `rgb2gray`. The result obtained from the greyscale transformation is subsequently shown in Figure 4.2.

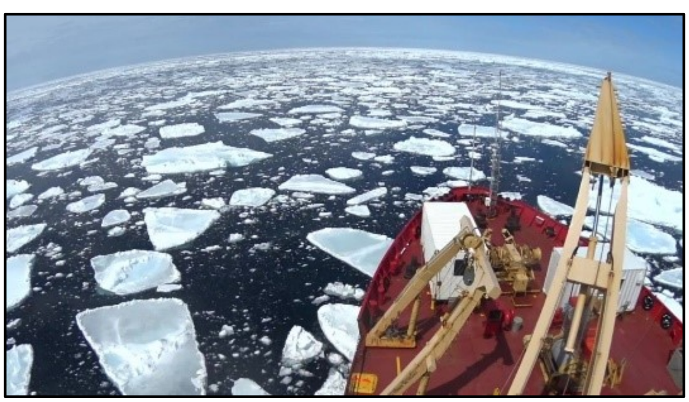

Figure 4.1 The test image from the Amundsen used for image processing analysis

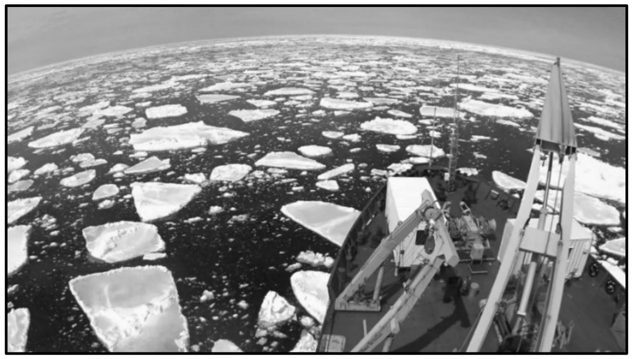

Figure 4.2 The greyscale image

The second step is to improve the quality of the image by enhancing the contrast. This ensures that as much detail as possible would be preserved throughout the processing steps. This is done by applying a MATLAB function known as `imadjust`. Figure 4.3 shows the result.

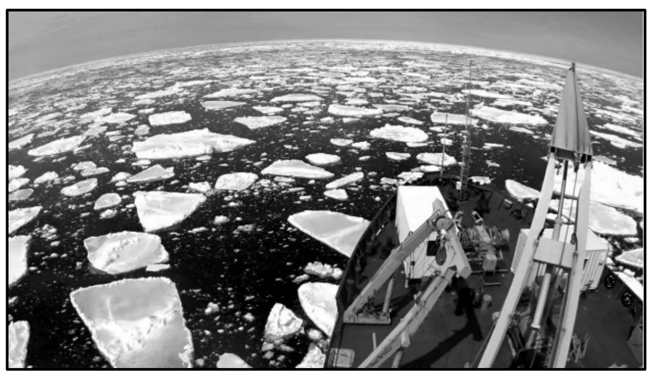

Figure 4.3 The example image used for analysis with enhanced contrast

4.1.2. Camera Lens Distortion Removal

The camera used for the image collection has a noticeable fisheye effect which helps it cover a wide angle of view. However, it also means that true scale is distorted. Thus, it is necessary to remove the effect of this distortion. The method and results of this processing step are described in the following sections.

4.1.2.1. Determination of Camera Parameters

From this step, the camera parameters are determined which are then used for the lens distortion removal in the second and fourth processing steps. Some of the important camera parameters are shown in the matrix below.

$$K = \begin{pmatrix} \frac{fx}{Sx} & 0 & cx \\ 0 & \frac{fy}{Sy} & cy \\ 0 & 0 & 1 \end{pmatrix}$$

$$K = \begin{pmatrix} 892 & 0 & 616 \\ 0 & 896 & 318 \\ 0 & 0 & 1 \end{pmatrix}$$

4.1.2.2. Distortion Removal

The result of this lens distortion removal is shown below in Figure 4.4 and compared against the original to highlight the difference. This change can be difficult to recognize without comparison. The horizon in the image serves as a good feature for comparison.

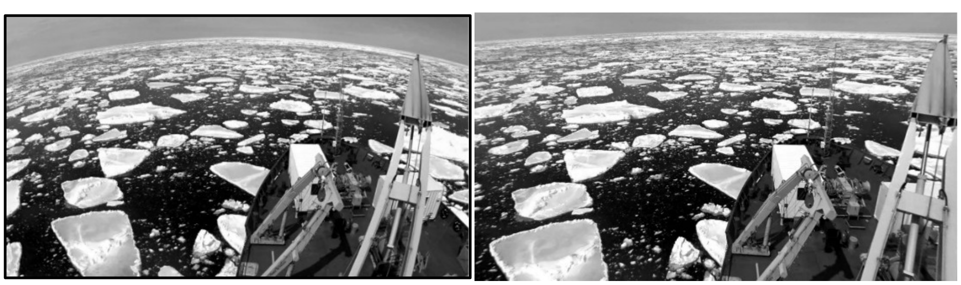

Figure 4.4 The original image (left) and the image after the distortion removal (right)

It is worth noting that some information is lost in the image due to this lens removal process, but the information is not overly significant as it is the information on the edges of the image.

4.1.3. Projective Transformation

The next step is the transformation of the imagery from a forward looking view to a top-down view which can then be used for analysis. Since the goal of the work is to augment the image with the vessel manoeuvrability parameters, the image needs to be in a perspective that would show the ocean surface plane. The result of this transformation is shown in Figure 4.5 below.

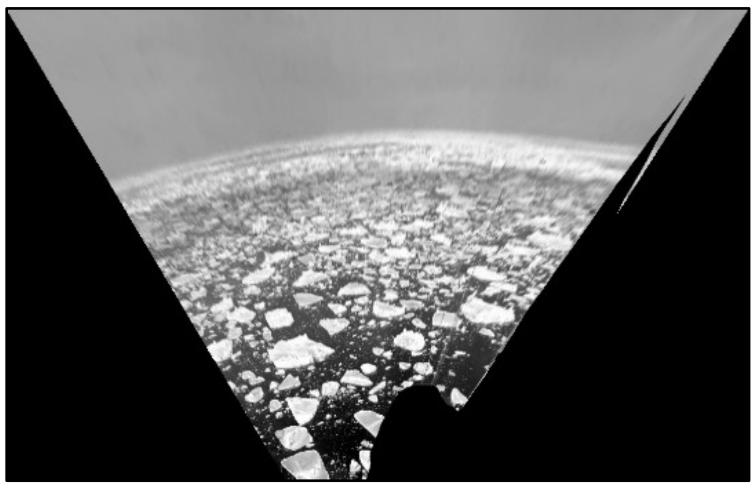

Figure 4.5 The transformation of the sea ice field view normal to the vessel's plane of travel

4.1.4. Image Enlargement for True Scale

To apply rescaling to the image, geometry calculations based on the height of the camera and reference features are used to determine the scale factors. The factors are applied to individual pixels in the forward direction to obtain the rescaled image. Because of the exponential increase in magnitude of scale factors at locations close to the horizon, the scale factors are standardized at a particular point. This is done to account for the memory limitations of MATLAB, which was used for processing.

The main function used for this rescaling step is the MATLAB function `repelem`. The region rescaled is between the horizontal lines labelled 0 to 300 below in Figure 4.6. Between lines at 300 and 360, the scale factors are limited to a magnitude of 30.

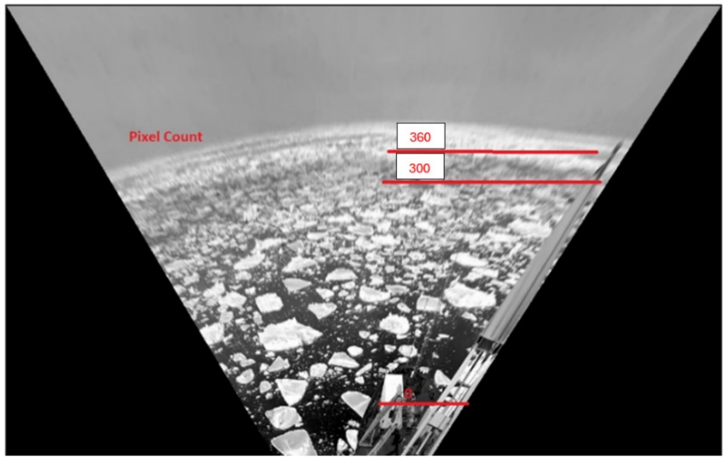

Figure 4.6 The region in the original image that is to be rescaled

To determine the scale factors to use for the rescaling of the image, some geometry calculations are carried out. A true scale image of the vessel is used to determine the distances shown in the images. The images used in the image enlargement methodology are shown below in Figure 4.7.

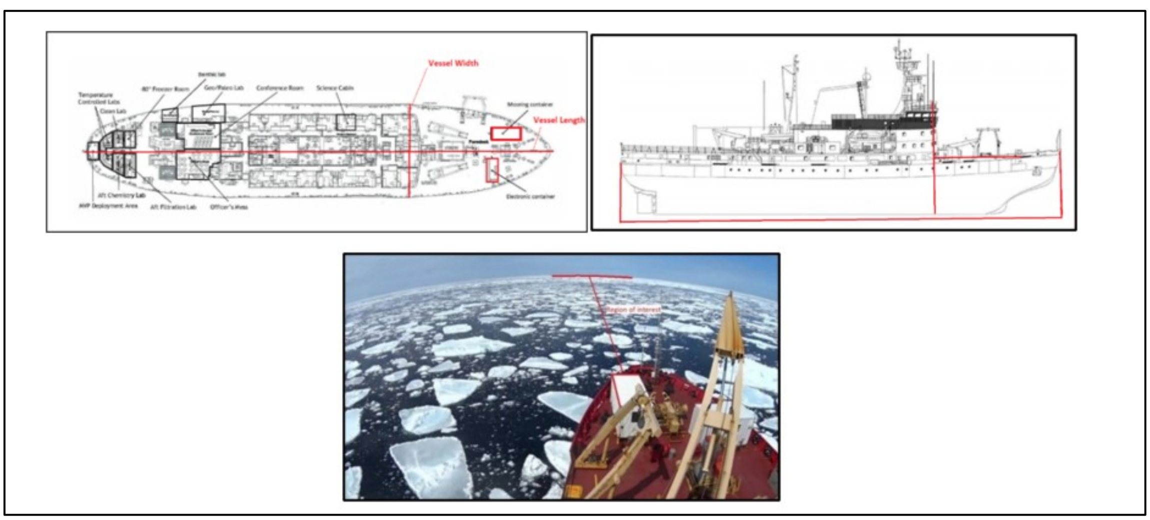

Figure 4.7 Related parameters used for the image enlargement pre-calculations

The parameters that are used for the pre-calculations are all noted in the Table 4.1. These are obtained from true scale diagrams of the given vessel.

Table 4.1 with reference distances used for image scale

Parameters	Values
Camera height above sea level	24.8m
Camera Height Above mooring container	12.4m
Distance from Camera to Mooring Container	15.4m
Distance from mooring container to horizon	17.96km
Angle to mooring container edge	51.3 deg
Angle to horizon	89.9 deg
Number of pixels between references	190
Degree Increments between references	0.204 deg

These parameters are then used to calculate scale factors that are applied to enlarge the image. The scale factors would be applied to each individual pixel. Below, Figure 4.8 shows the scale factors with the corresponding pixel count.

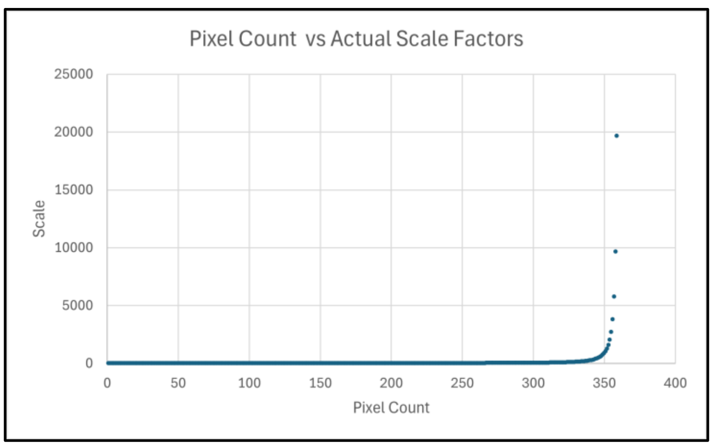

Figure 4.8 Pixel count vs the actual unchanged scale factors

It is evident from Figure 4.8 that the scale factors maintain a very low value until around the 340th pixel where the value rises significantly. This posed a significant problem in processing as the number of elements needed to apply the scale factors rose as high as 20000. Performing this task demanded a significant amount of computer memory and so a cutoff point was identified to allow for the enlargement of the portion of the image where the scale factors were still within an acceptable range. This range was calculated to be around a scale factor magnitude of 30. Figure 4.9 below shows these new scale factors with a cutoff of 30, above which the scale factor is held constant. This helped to limit memory requirement for the image processing.

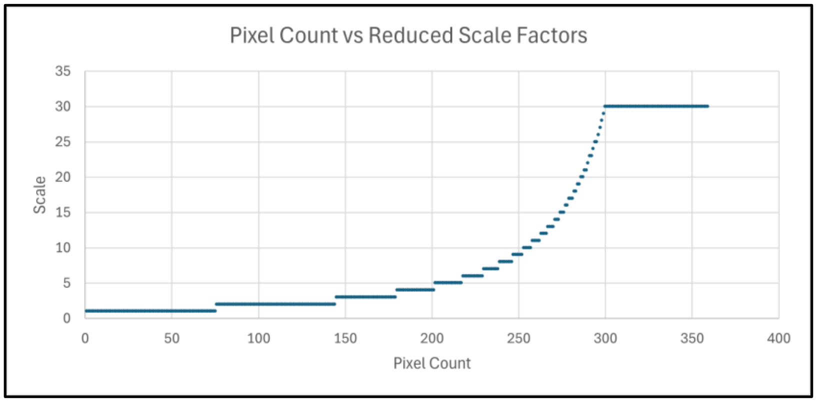

Figure 4.9 The scale factors with a limit of a magnitude of 30

After obtaining the relevant scale factors, the image enlargement is carried out and the subsequent result is shown in Figure 4.10.

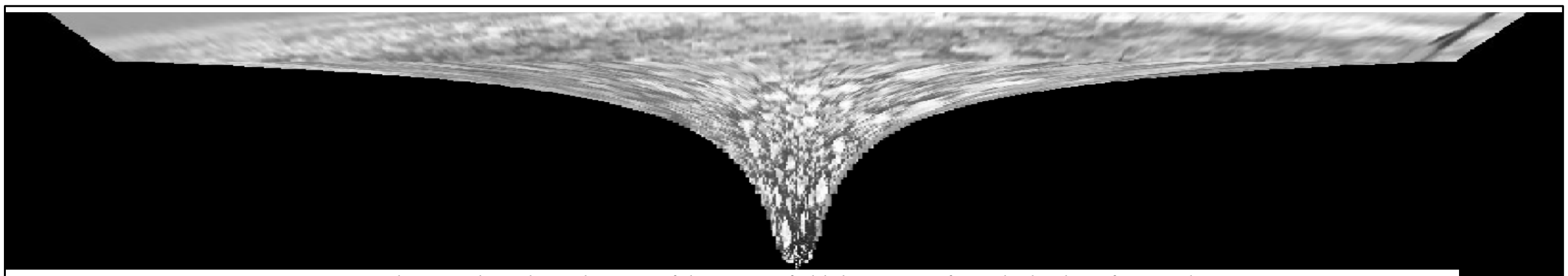

Figure 4.10 showing the enlarged image of the sea ice field that is seen from the bridge of a vessel.

Due to the limitation of the scale factors to a magnitude of 30 at the horizontal pixel line of around 300 as shown in Figure 4.9, the detail shown in the image will be limited. It is important to note however, that features in the images become significantly distorted around the 300^{th} pixel region and beyond.

4.2. Stopping Distance and Turning Circle Parameters

The stopping distance and turning circle parameters are also calculated for a range of values for the three sample vessels. The results are shown in Tables 4.2 to 4.5.

Vessel Speed 1: 11 knots

Table 4.2 showing the results for the manoeuvrability parameter calculation at 11 knots

Parameter (ship lengths)	Sample Vessel 1	Sample Vessel 2	Sample Vessel 3
Length (m)	98	189	350
Stopping Distance Method 1	3.32 to 4.71	2.25 to 3.64	3.66 to 5.61
Stopping Distance Method 2	6.05	6.29	4.61
Advance	3.64	4.19	2.95
Transfer	2.14	2.68	1.48

Vessel Speed 2: 8 knots

Table 4.3 showing the results for the manoeuvrability parameter calculation at 8 knots

Parameter (ship lengths)	Sample Vessel 1	Sample Vessel 2	Sample Vessel 3
Length (m)	98	189	350
Stopping Distance Method 1	3.32 to 4.71	2.25 to 3.64	3.66 to 5.61
Stopping Distance Method 2	4.40	4.56	3.35
Advance	3.57	4.15	2.91
Transfer	2.08	2.63	1.45

Vessel Speed 3: 5 knots

Table 4.4 showing the results for the manoeuvrability parameter calculation at 5 knots

Parameter (ship lengths)	Sample Vessel 1	Sample Vessel 2	Sample Vessel 3
Length (m)	98	189	350
Stopping Distance Method 1	3.32 to 4.71	2.25 to 3.64	3.66 to 5.61
Stopping Distance Method 2	2.75	2.86	2.09
Advance	3.51	4.09	2.88
Transfer	2.02	2.59	1.42

Vessel Speed 4: 3 knots

Table 4.5 showing the results for the manoeuvrability parameter calculation at 3 knots

Parameter (ship lengths)	Sample Vessel 1	Sample Vessel 2	Sample Vessel 3
Length (m)	98	189	350
Stopping Distance Method 1	3.32 to 4.71	2.25 to 3.64	3.66 to 5.61
Stopping Distance Method 2	1.65	1.71	1.26
Advance	3.46	4.06	2.86
Transfer	1.97	2.55	1.39

These manoeuvrability values are then augmented with the enlarged images to give a visual image showing an operational area of relevance of the ice field bounded by the Turning Circle and Stopping Distance parameters. A sample of the results of the image augmentations is shown for the Sample 1 Vessel in the following section. It should be noted that Method 2 was used for the Stopping Distance since it reflects the impact of vessel speed in its calculations.

4.3. Image Augmentation Sample Results

Once the manoeuvrability parameters are determined, they are combined with the transformed and enlarged images to create a visual representation of the operational area of relevance, defined by the Turning Circle and Stopping Distance parameters. Method 2 was used for the Stopping Distance, as it accounts for the impact of vessel speed in its calculations. The results of this process, including the integration of the Stopping Distance, Advance, and Transfer parameters with the transformed images, are presented for Sample Vessel 1 in the following section. Figure 4.11 shows the results for Sample Vessel 1 at a speed of 11 knots.

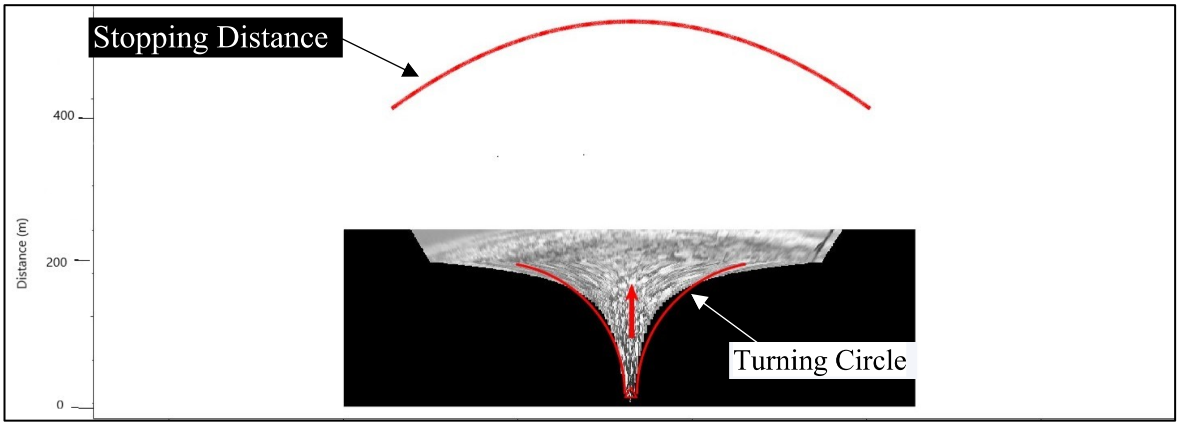

Figure 4.11 The stopping distance and turning circle boundaries for the Sample 1 Vessel at 11 knots

A similar result can be shown in Figure 4.12 for the same vessel for a speed of 3 knots.

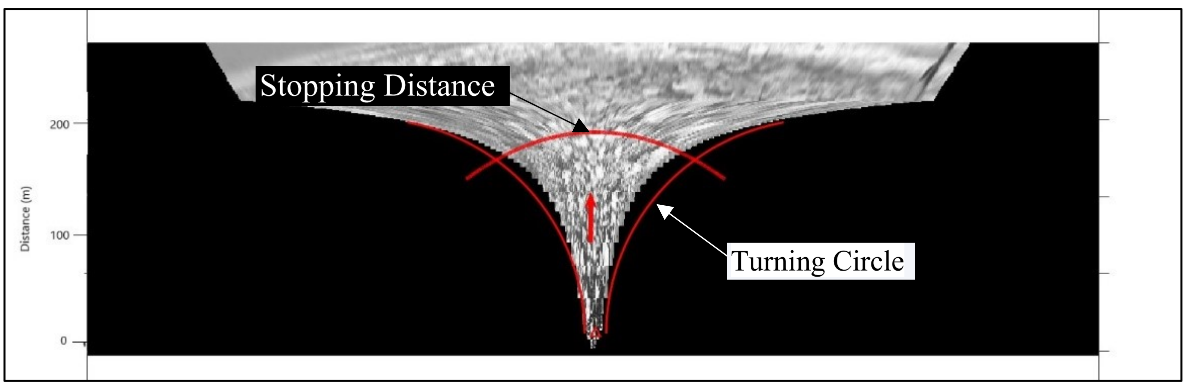

Figure 4.12 The stopping distance and turning circle boundaries for the Sample 1 vessel at 3 knots

4.4. Chapter Conclusion

This chapter presents the results of the image processing procedure, including the augmentation of the processed images with manoeuvrability values corresponding to the POLARIS-recommended vessel speeds. The outcomes of the different methods used to calculate stopping distance and turning circle values are also detailed. Finally, a case study is provided for a sample vessel traveling at a speed of 8 knots, where the stopping distance and turning circle are overlaid on a transformed image to illustrate the extent of the manoeuvrability parameters within the sea ice field.

Chapter 5: Analysis

This section seeks to highlight the implications of the results obtained in Chapter 4. The aim is to highlight that factors other than ice conditions and vessel ice class can affect a vessel's hazard avoidance techniques. This will be illustrated by a test case scenario in which an example hazard is placed in front of the vessel. The hazard will be at a distance close to the extent of the image augmentation where features can easily be made out (i.e., around the 300th pixel). Two different vessels assumed to be in the same Polar Class are used to highlight how vessels within the same ice classification will have different hazard avoidance options.

The test case involves an ice hazard which is 50m in diameter and is 175m directly ahead of the vessel in question. Beyond this point, the ice features are overly distorted and difficult to make out. Two vessels with the properties shown in Table 5.1 will be used for three speed recommendations from the POLARIS classification. These include the PC2 at 8 knots, PC3-PC5 at 5 knots and Below PC5 at 3 knots. These are shown in the table below and the corresponding parameters are also shown.

Table 5.1 showing the properties of the two vessels used for analysis

Sample Vessel	Length L (m)	Breadth B (m)	Draft (m)	Mass (metric tons)
Vessel 1	98	19.5	7.2	5911
Vessel 2	189	26.6	11.7	22 462

The speed recommendation of 11 knots for the PC1 class was not used in this analysis. This is because the vessels in this class are designed to operate all year round in all polar waters. Thus, the analysis was carried out for the remaining three speed recommendations.

Calculations were carried out for the vessels for the various speeds, and these are shown in the two tables Table 5.2 and Table 5.3. These show the results for the various manoeuvrability parameters for both vessels.

Table 5.2 showing results for Vessel 1, an icebreaker with length 98m

Polar Class	Speed	Stopping Distance (ship lengths)	Advance (ship lengths)	Transfer (ship lengths)
PC1	11 knots	6.05	3.64	2.14
PC2	8 knots	4.40	3.57	2.08
PC3-PC5	5 knots	2.75	3.51	2.02
Below PC5	3 knots	1.65	3.46	1.97

Table 5.3 showing results for Vessel 2, a bulk carrier with length 189m

Polar Class	Speed	Stopping Distance (ship lengths)	Advance (ship lengths)	Transfer (ship lengths)
PC1	11 knots	6.28	4.19	2.68
PC2	8 knots	4.55	4.15	2.63
PC3-PC5	5 knots	2.86	4.09	2.59
Below PC5	3 knots	1.71	4.06	2.55

Once the parameters were determined, the augmentation with the test case scenario of a hazard on the image was depicted for the two vessels. This is shown in the following sections.

5.1. Case Study: Ice Hazard Ahead of Vessel

The analysis carried in this section contrasts two different vessels with different stopping distance and turning circle parameters. The results of the analysis will be shown in terms of image augmented with the stopping distance and turning circle boundaries when confronted with the test case of an ice hazard of 50m diameter, and at a distance of 175m straight ahead

5.1.1. Vessel Speed of 8 knots

For vessels in this category, the maximum recommended speed is 8 knots, therefore an analysis was carried out using this speed for the two vessels. Figures 5.1 and 5.2 show the results.

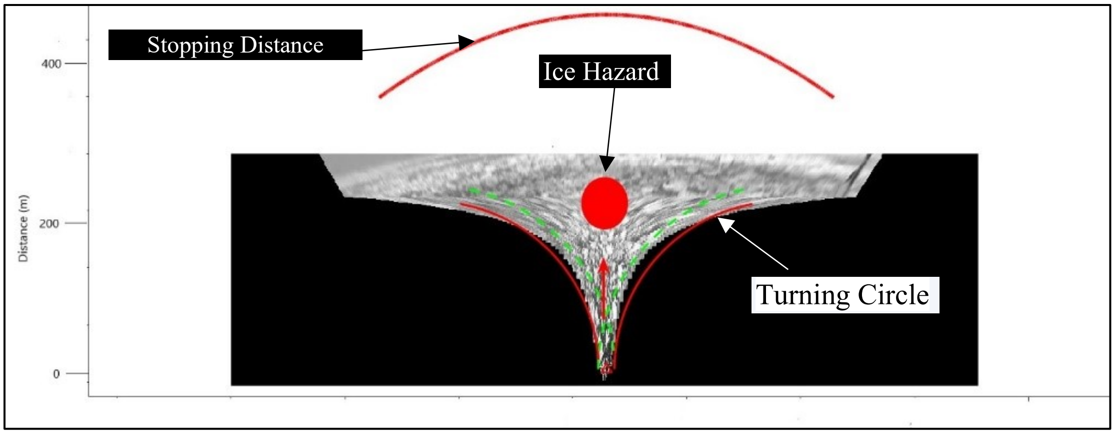

Figure 5.1 The boundaries for Sample Vessel 1 at 8 knots

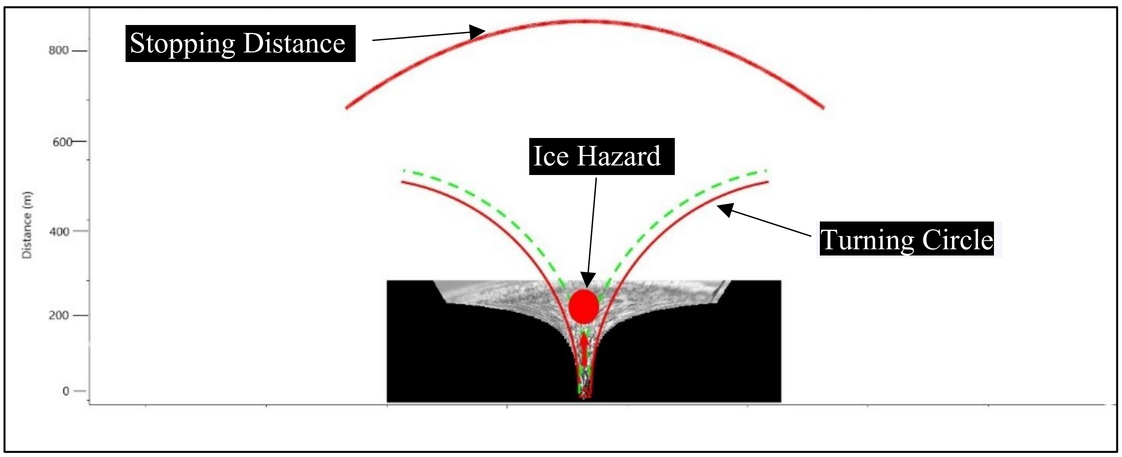

Figure 5.2 The boundaries for Sample Vessel 2 at 8 knots

Figure 5.2 above shows the results for Sample Vessel 1, an icebreaker of length 98m treated as a Polar Class 2 with a speed recommendation of 8 knots. As can be seen in the image, the stopping distance boundary is much farther than the ice hazard region and it is beyond the extent to which the camera provides useful information. On the other hand, the turning circle parameters show that an extreme port side or starboard turn would be a sufficient measure to avoid the hazard.

For Sample Vessel 2, a bulk carrier of length 189m with the same Polar Class PC2 and speed of 8 knots, it is evident as well that the stopping distance is well beyond the ice hazard and the extent of the useful information shown in the image. This is similar to the first case with Sample Vessel 1, and consequently a stopping manoeuvre would not be the best measure to avoid the hazard. As for the turning circle parameters, it is evident that an extreme starboard or port side turn would not lead to full avoidance of the obstacle. This is an indication that for certain lengths of vessels, manoeuvrability is extremely limited to the point that impact with hazards in some cases would be inevitable. It also shows that in some cases, visual systems may not be the best means to monitor for ice hazards where the primary way to deal with them would be avoidance.

5.1.2. Vessel Speed of 5 knots

For the scenario of PC 3-5, the maximum speed recommended is 5 knots and thus the corresponding stopping distance and turning circle boundaries are shown in the Figures 5.3 and 5.4 for the two sample vessels.

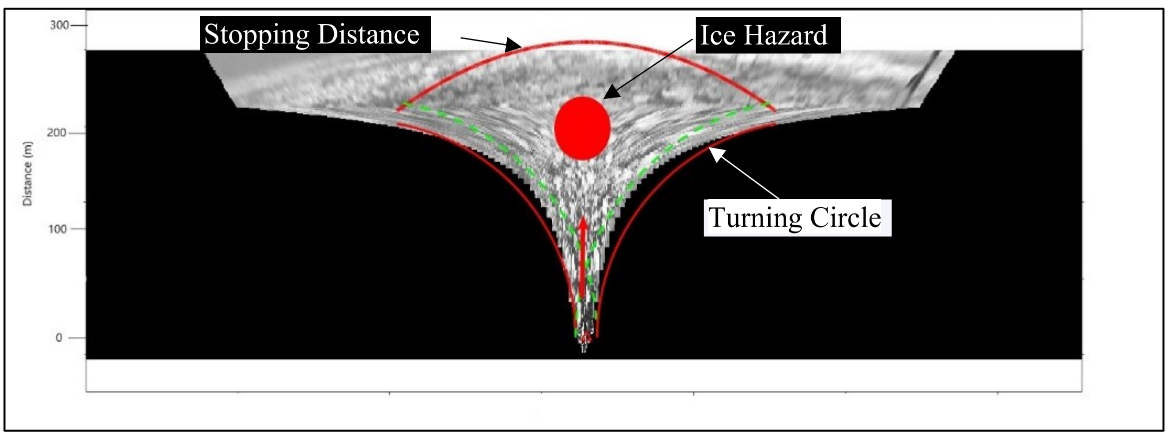

Figure 5.3 The boundaries for Sample Vessel 1 at 5 knots

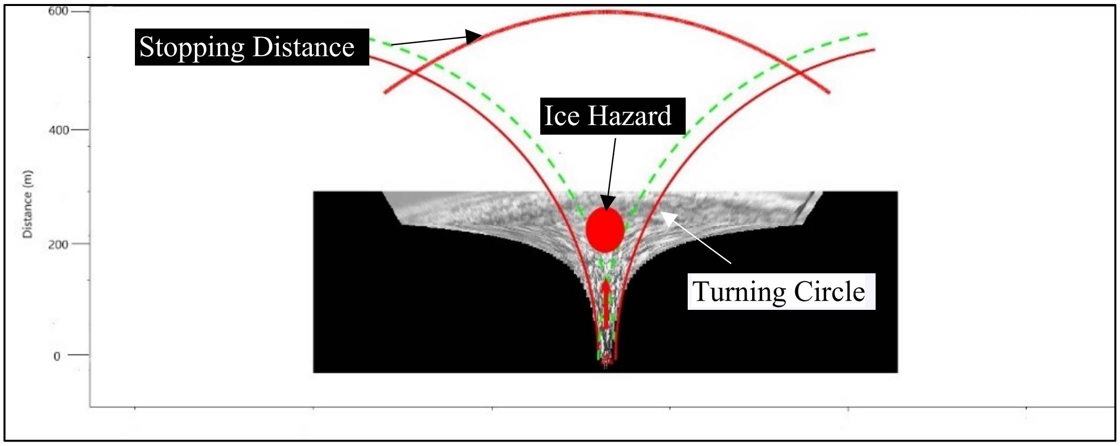

Figure 5.4 The boundaries for Sample Vessel 2 at 5 knots

Similar to the results shown for the PC2 speed recommendation of 8 knots, the boundaries for the two vessels highlight the same capabilities and limitations. First, it is clear that both vessels are unable to use the stopping manoeuvre as an option to avoid the ice hazard region, while Sample Vessel 1 shows the capability to turn port side or starboard as a possible means of hazard avoidance. This observation further highlights that those two different vessels, assumed to be in the same Polar Class and operating under the same ice conditions, would have different areas of interest for tactical navigation and different options for avoiding hazards. These operational differences need to be recognized when considering onboard cameras for decision support for navigation.

5.1.3. Vessel Speed of 3 knots

For the scenario of vessels below PC5, the maximum speed recommendation is 3 knots and the results are shown in the Figures 5.5 and 5.6.

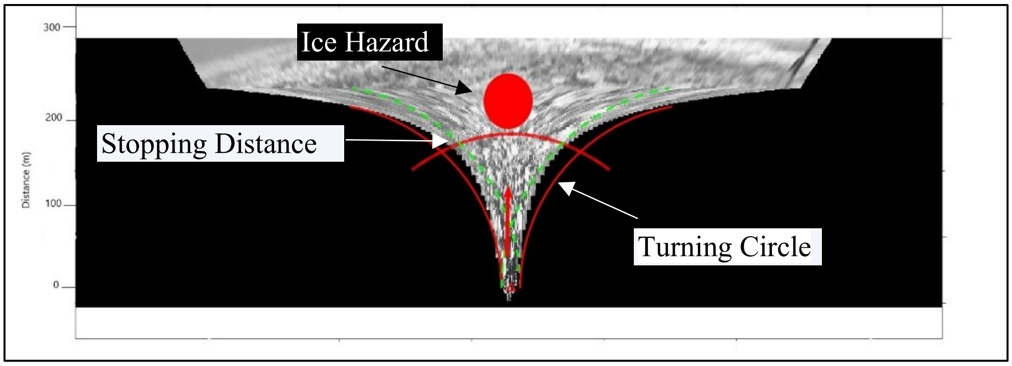

Figure 5.5 The boundaries for Sample Vessel 1 at 3 knots

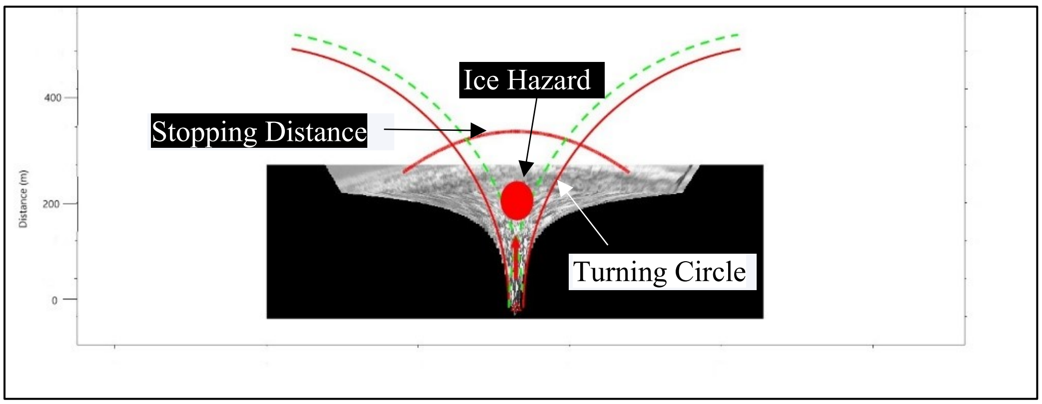

Figure 5.6 The boundaries for Sample Vessel 2 at 3 knots

For this category, we can see that Sample Vessel 1 has more options in terms of hazard avoidance. First, the ice hazard is in a region that is outside its stopping distance boundary, highlighting the possibility for it to use the stopping manoeuvre to avoid the hazard. In addition, it still has the option of turning as an avoidance strategy. On the other hand, Sample Vessel 2 still has the same limitations as it had for the 8 and 5 knots speed recommendations.

The results in this analysis show varying boundaries for the Stopping Distances and Turning Circle parameters for two vessels that were assumed to be of the same ice class, highlighting the importance of incorporating vessel properties when assessing risk posed by ice hazards and determining avoidance strategies. Further discussion of the implications of the analysis is presented in the sections below.

5.2. Stopping Distance

The use of stopping to avoid hazards for the two vessels does not appear to be effective in most cases except in the Polar Classes below PC5 where the recommended maximum speed is 3 knots, and even then, it is only for the Sample Vessel 1. For Sample Vessel 2, which has the same Polar Class but with almost double the length of Vessel 1, the stopping manoeuvre is not effective for avoiding the same hazard.

In the study and as was shown in Chapter 4, the stopping distance changes significantly with each Polar Class speed recommendation, highlighting the strong relationship between the stopping distance and the vessel speed. This relationship was emphasized by the linear relationship shown between the stopping distance and the vessel speed in Figure 3.19 in Chapter 3. The implication from this is that the vessel's operational conditions will have an effect on a vessel's capability to navigate in waters where it could encounter hazards that would require stopping or turning. Operating at lower speeds in such regions would seem to favour a smaller unavoidable area of navigable relevance, improving safety of vessel operations.

5.3. Turning Circle

In terms of the Turning Circle, Sample Vessel 1 had the option of turning to avoid the ice hazard for all three speed recommendations. This highlights the fact that the speed did not significantly affect the turning circle parameters of Transfer and Advance. Sample Vessel 2 had higher values for its turning circle parameters which meant that for all Polar Class designations, turning port-side or starboard would not have led to hazard avoidance. This highlights the limitation that longer vessels have in terms of turning to avoid hazards. A key takeaway from this is also that the vessel length has a significant bearing on the turning ability of a vessel.

It is worth noting that the values of the Transfer and Advance parameters did not change significantly throughout the analysis for both vessels in all the Polar Class speed recommendations. For the Transfer parameter, Sample Vessel 1 had a change from 3.64 ship lengths at 11 knots to 3.46 ship lengths at 3 knots, representing a 3% decrease. Sample Vessel 2 also had a 3% decrease from 4.19 to 4.06 ship lengths with the same speed reduction from 11 knots to 3 knots. Similarly, for the Transfer parameter, Sample Vessel 1 had an 8% decrease from 2.14 to 1.97 ship lengths, while Vesel B had a 5% decrease from 2.68 to 2.55 ship lengths. These low values are consistent with the observation that the turning capability does not change significantly throughout the various Polar Class speed recommendations.

5.4. Performance of Onboard Camera Systems

As can be seen from the results, the area of operational significance for a given vessel is shown to exceed the range at which an onboard camera can effectively detect and characterize ice features at a level useful enough for tactical navigation. The images shown for the two sample vessels highlight this limitation, as most manoeuvrability parameter boundaries in the image exceeded the scope of the captured image. Indeed, the only results from the analysis that had all the boundaries in the scope of the image was the image for Sample Vessel 1 at the lowest speed rating of 3 knots.

In addition to this limitation, it was also evident from the Image Enlargement Processing Step that though the onboard camera shows the scope of the ice field from the bow of the vessel to the horizon, the ice features in the field become blurry and indistinguishable at a particular point in the image as information is condensed in the image. For the analysis carried out in this work, the point in the image where this transition occurs appears to be around 175m to 200m ahead of the vessel. The detection of hazardous ice features would be challenging at these distances.

The conclusions obtained from the foregoing analysis are presented in the next chapter.

Chapter 6: Conclusion

From the previous chapters outlining the methodologies, results and the analysis of a test case scenario, the following conclusions can be made:

6.1. Main Study Conclusions

The following main points can be deduced from the work presented in this study.

1. Firstly, the methodology employed in this research successfully integrated vessel properties and performance parameters to illustrate a vessel's hazard avoidance options under certain operational conditions

The image projective transformation methods were successfully employed to process an image of the sea ice field to one that can visually illustrate a vessel's capabilities in ice hazard avoidance under various speed recommendations. This was an image, shown in Figure 4.12 that can easily be interpreted onboard vessels and shows promise in its practical utility for vessel tactical navigation

2. Secondly, the use of POLARIS to assess vessel suitability for specific ice conditions in tactical navigation is limited. It is important that vessel properties are taken into consideration when deciding to support operations for vessels in ice conditions.

This is because vessels within the same ice class operating under identical ice conditions can exhibit differing manoeuvrability due to variations in vessel properties. These differences may affect a vessel's ability to employ avoidance techniques when navigating ice hazards. The analysis chapter highlights this issue by illustrating different operational parameters for two vessels of the same Polar Class but of differing lengths, underscoring the impact of vessel length on vessel tactical navigation. From the calculations of stopping distance and turning circle, it was shown that initial vessel speed generally has a linear directly proportional relationship with stopping distance, while the turning circle is primarily influenced by vessel length, with vessel speed having minimal impact.

3. The onboard cameras utilized in this work show limited operational utility in supporting tactical navigation decision making for wider operational areas.

The results from the processing the camera images showed that the final images did not fully encompass the stopping distance and turning circle boundaries for most vessel cases. This illustrates a significant limitation that the onboard camera's field of view did not fully cover the operational boundaries defined by the stopping distance and turning circle parameters. This is a common challenge for onboard cameras. Additionally, the image quality deteriorated at distances beyond 175 meters, making it difficult to distinguish image details. This highlights the significant limitation of relying solely on onboard cameras for ice monitoring and hazard avoidance and emphasizes the need for supplementary tools such as radar and LIDAR for effective ice hazard detection for far field ice feature monitoring.

Going forward, onboard cameras should ideally have a range that aligns with the vessel's stopping distance and turning circle parameters. This ensures that the entire operational area is covered in sea ice field analyses for effective hazard avoidance planning. For example, the vessels examined in this study would require a camera range of at least 1,600 meters forward and 500 meters laterally to fully capture the boundaries of their stopping distance and turning circle parameters. These values are derived from Figures 3.19, 3.21 and 3.23.

Beyond the conclusions drawn in this study, there are additional aspects that warrant further investigation to reinforce some of the findings outlined here, which were beyond the scope of this project. These areas for future research are discussed in the next section.

6.2. Areas for Further Work

A significant portion of this project focused on image processing to generate images that could be augmented with manoeuvrability parameters. This process offers opportunities for further refinement. For instance, the ability to distinguish ice features was limited to a range of approximately 175–200m ahead of the vessel. Future work could explore methods to extract more detailed information from images captured by onboard cameras. One potential avenue is the use of advanced computer hardware with sufficient memory capacity to handle the large scale factors required during the image rescaling step in the transformation process.

High-resolution cameras capable of capturing detailed far-field ice features could be used for data collection and analyzed with more computationally intensive algorithms. This represents a potential area for development, where integrating such technology with marine systems could enhance the analysis and interpretation of far-field ice features. As was indicated in the conclusion, the required range of the cameras needs to be in line with the stopping distance and turning circle boundaries and the use of more advanced cameras that have higher resolutions for far-field ice features would be extremely useful.

Additionally, the manoeuvrability parameters in this study were derived from calculations based on vessel properties obtained from publicly available data. These calculations could be improved by incorporating data from actual sea trials of the stopping distance and turning circle tests. Such data would help validate the findings of this study.

From a practical perspective, there is a need to also develop methodologies that can easily provide information to navigators in a timely manner and format that will aid in tactical navigation decision making. Perhaps the analysis of real time footage could be carried to assist navigators with real time ice hazard identification to help optimize vessel performance in ice.

Moreover, other vessel properties, such as weight and block coefficient, may influence the stopping distance and turning circle parameters. Investigating the effects of these properties on vessel manoeuvrability could further enhance understanding in this area

Bibliography

1. Sabir, Aneela, et al. "Impact of CO 2 discharge from distilleries on climate changes: key facts." *Sustainable ethanol and climate change: sustainability assessment for ethanol distilleries* (2021): 113-140.
2. Adolph, Marie-Luise, et al. "North Atlantic Oscillation polarity during the past 3000 years derived from sediments of a large lowland lake, Schweriner See, in NE Germany." *Climate of the Past* 20.9 (2024): 2143-2165.
3. Bigg, Grant R., and Mattias Green. "Has the impact of the Earth's orbital variation at sub-myriadal timescales been underestimated?" (2023).
4. Randell, Charles, et al. "SS: Canadian: Atlantic development; technological advances to assess, manage and reduce ice risk in northern developments." *Offshore Technology Conference*. OTC, 2009.
5. Keinonen, Arno Juhani. "Ice Management for Floating Ice Offshore Operations." *Offshore Technology Conference*. OTC, 2008.
6. Hamilton, Jed M., Curtis Holub, and Joshua Blunt. "Simulation of ice management fleet operations using two decades of Beaufort Sea ice drift and thickness time histories." *ISOPE International Ocean and Polar Engineering Conference*. ISOPE, 2011.
7. Kooij, Carmen, and Robert Hekkenberg. "Towards unmanned cargo-ships: the effects of automating navigational tasks on crewing levels." *Available at SSRN 3438144* (2019).
8. Ruiz-De-Azúa, Joan A., Adriano Camps, and Anna Calveras Augé. "Benefits of using mobile ad-hoc network protocols in federated satellite systems for polar satellite missions." *IEEE access* 6 (2018): 56356-56367.

9. Neville, M. A., F. Scibilia, and E. H. Martin. "Physical Ice Management Operations-Field Trials and Numerical Modeling." *OTC Arctic Technology Conference*. OTC, 2016.
10. McKenna, Richard, Walt Spring, and Graham Thomas. "Use of the ISO 19906 Arctic Structures Standard." *OTC Arctic Technology Conference*. OTC, 2011.
11. Shokr, Mohammed, and Nirmal K. Sinha. Sea Ice. John Wiley & Sons, 2023. Toomey, Patrick. "Ice Navigation and the -Electronic Age." www.hydro-International.com, 18 Jan. 2015
12. Zhou, Li, Jinyan Cai, and Shifeng Ding. "The identification of ice floes and calculation of sea ice concentration based on a deep learning method." *Remote Sensing* 15.10 (2023): 2663.
13. Bhardwaj, Anshuman, et al. "LiDAR remote sensing of the cryosphere: Present applications and future prospects." *Remote Sensing of Environment* 177 (2016): 125-143.
14. Randell, Charles, et al. "Satellite-based ice and iceberg monitoring for offshore engineering design and tactical operations." *Offshore Technology Conference*. OTC, 2011.
15. Panchi, Nabil, Ekaterina Kim, and Anirban Bhattacharyya. "Supplementing remote sensing of ice: Deep learning-based image segmentation system for automatic detection and localization of sea-ice formations from close-range optical images." *IEEE Sensors Journal* 21.16 (2021): 18004-18019.
16. Fedi, Laurent, et al. "Arctic navigation: stakes, benefits and limits of the POLARIS system." *The Journal of Ocean Technology* 13.4 (2018): 54-67.
17. Lu, Peng, and Zhijun Li. "A method of obtaining ice concentration and floe size from shipboard oblique sea ice images." *IEEE Transactions on geoscience and remote sensing* 48.7 (2010): 2771-2780.

18. Zhang, Qin, et al. "Digital image processing for sea ice observations in support to Arctic DP operations." *International Conference on Offshore Mechanics and Arctic Engineering*. Vol. 44939. American Society of Mechanical Engineers, 2012.

19. Peng, Liran, et al. "Role of intense Arctic storm in accelerating summer sea ice melt: An in situ observational study." *Geophysical Research Letters* 48.8 (2021): e2021GL092714.

20. Zhang, Qin, and Roger Skjetne. "Image processing for identification of sea-ice floes and the floe size distributions." *IEEE Transactions on geoscience and remote sensing* 53.5 (2014): 2913-2924.

21. Maritime Safety Committee. *Guidance on methodologies for assessing operational capabilities and limitations in ice*. Tech. Rep. MSC. 1/Circ. 1519, International Maritime Organization, London. 2016. https://www. nautinst. org/uploads/assets/uploaded/2f01665c-04f7-4488-802552e5b5db62d9. pdf, 2016.

22. Government of Canada. "Manual of Ice (MANICE) - Canada.ca." *Canada.ca*, 2016, *www.canada.ca/en/environment-climate-change/services/weather-manuals-documentation/manice-manual-of-ice.html*. Accessed 20 Nov. 2024

23. Howell, Stephen EL, Claude R. Duguay, and Thorsten Markus. "Sea ice conditions and melt season duration variability within the Canadian Arctic Archipelago: 1979–2008." *Geophysical Research Letters* 36.10 (2009).

24. Canadian Ice Service. "Ice Navigation in Canadian Waters." *Fisheries and Oceans Canada* Aug. 2012, *https://waves-vagues.dfo-mpo.gc.ca/Library/347665.pdf.* Accessed 21 Feb. 2025

25. International Maritime Organization (IMO). *International Code For Ships Operating In Polar Waters (Polar Code)* MEPC 68/21 Add. 1 Annex, London UK, 2015

26. Henriksen, Tore. "Protecting polar environments: Coherency in regulating Arctic shipping." *Research handbook on international marine environmental law*. Edward Elgar Publishing, 2015. 363-384.

27. Fedi, Laurent, Olivier Faury, and Daria Gritsenko. "The impact of the Polar Code on risk mitigation in Arctic waters: a "toolbox" for underwriters?." *Maritime Policy & Management* 45.4 (2018): 478-494.

28. Dierking, Wolfgang. "Sea ice monitoring by synthetic aperture radar." *Oceanography* 26.2 (2013): 100-111.

29. Sillitoe, A., et al. "Supporting human performance in ice and cold conditions." *Lloyd's Register, London* (2010).

30. Yan, Wai Yeung, Ahmed Shaker, and Nagwa El-Ashmawy. "Urban land cover classification using airborne LiDAR data: A review." *Remote sensing of environment* 158 (2015): 295-310.

31. Worby, Anthony P., and Josefino C. Comiso. "Studies of the Antarctic sea ice edge and ice extent from satellite and ship observations." *Remote sensing of environment* 92.1 (2004): 98-111.

32. Wiebe, Heidrun, Georg Heygster, and Thorsten Markus. "Comparison of the ASI ice concentration algorithm with Landsat-7 ETM+ and SAR imagery." *IEEE Transactions on Geoscience and Remote Sensing* 47.9 (2009): 3008-3015.

33. Pang, Xiaoping, et al. "Comparison between AMSR2 sea ice concentration products and pseudo-ship observations of the Arctic and Antarctic sea ice edge on cloud-free days." *Remote Sensing* 10.2 (2018): 317.

34. Wagner, Penelope Mae, et al. "Sea-ice information and forecast needs for industry maritime stakeholders." *Polar Geography* 43.2-3 (2020): 160-187.

35. Huang, Wenjun, et al. "Sea Ice Extraction via Remote Sensing Imagery: Algorithms, Datasets, Applications and Challenges." *Remote Sensing* 16.5 (2024): 842.
36. Agarwal, Neeraj, et al. "Geostationary satellite-based observations for ocean applications." *Current Science* 117.3 (2019): 506-515.
37. Rinne, E., and M. Similä. "Utilisation of CryoSat-2 SAR altimeter in operational ice charting." *The Cryosphere* 10.1 (2016): 121-131.
38. Mäkynen, Marko, and Juha Karvonen. "Incidence angle dependence of first-year sea ice backscattering coefficient in Sentinel-1 SAR imagery over the Kara Sea." *IEEE Transactions on Geoscience and Remote Sensing* 55.11 (2017): 6170-6181.
39. Eriksson, Leif EB, et al. "Evaluation of new spaceborne SAR sensors for sea-ice monitoring in the Baltic Sea." *Canadian Journal of Remote Sensing* 36.sup1 (2010): S56-S73.
40. Earth Science Data Systems, NASA. "Earthdata." *Earthdata*, (2019), www.earthdata.nasa.gov/learn/backgrounders/what-is-sar.
41. Arnold, N. S., et al. "Evaluating the potential of high-resolution airborne LiDAR data in glaciology." *International Journal of Remote Sensing* 27.6 (2006): 1233-1251.
42. Dierking, Wolfgang, Oliver Lang, and Thomas Busche. "Sea ice local surface topography from single-pass satellite InSAR measurements: a feasibility study." *The Cryosphere* 11.4 (2017): 1967-1985.
43. Comiso, Josefino C., et al. "Accelerated decline in the Arctic sea ice cover." *Geophysical research letters* 35.1 (2008).
44. Melsheimer, Christian, et al. "First results of Antarctic sea ice type retrieval from active and passive microwave remote sensing data." *The Cryosphere* 17.1 (2023): 105-126.

45. Ivanova, Natalia, et al. "Satellite passive microwave measurements of sea ice concentration: An optimal algorithm and challenges." *Cryosphere* 9.1 (2015): 1797-1817.

46. Kwok, R., et al. "Surface height and sea ice freeboard of the Arctic Ocean from ICESat-2: Characteristics and early results." *Journal of Geophysical Research: Oceans* 124.10 (2019): 6942-6959.

47. Maffezzoli, Niccolò, et al. "Sea ice in the northern North Atlantic through the Holocene: Evidence from ice cores and marine sediment records." *Quaternary Science Reviews* 273 (2021): 107249.

48. Wadhams, Peter, Nick Hughes, and João Rodrigues. "Arctic sea ice thickness characteristics in winter 2004 and 2007 from submarine sonar transects." *Journal of Geophysical Research: Oceans* 116.C8 (2011).

49. Doble, Martin J., et al. "The relation between Arctic sea ice surface elevation and draft: A case study using coincident AUV sonar and airborne scanning laser." *Journal of Geophysical Research: Oceans* 116.C8 (2011).

50. Bliss, Angela C., Jennifer K. Hutchings, and Daniel M. Watkins. "Sea ice drift tracks from autonomous buoys in the MOSAiC Distributed Network." *Scientific Data* 10.1 (2023): 403.

51. Alekseeva, Marina B. "Systemic diagnostics of the Arctic industry development strategy." *Записки Горного института* 238 (2019): 450-458.

52. Barnes, David KA, et al. "Icebergs, sea ice, blue carbon and Antarctic climate feedbacks." *Philosophical Transactions of the Royal Society A: Mathematical, Physical and Engineering Sciences* 376.2122 (2018): 20170176.

53. Weissling, B., et al. "EISCAM—Digital image acquisition and processing for sea ice parameters from ships." *Cold Regions Science and Technology* 57.1 (2009): 49-60.

54. Dowden, Benjamin, et al. "Sea ice classification via deep neural network semantic segmentation." *IEEE Sensors Journal* 21.10 (2020): 11879-11888.

55. Wright, Nicholas C., and Chris M. Polashenski. "Open-source algorithm for detecting sea ice surface features in high-resolution optical imagery." *The Cryosphere* 12.4 (2018): 1307-1329.

56. Panchi, Nabil, Ekaterina Kim, and Anirban Bhattacharyya. "Supplementing remote sensing of ice: Deep learning-based image segmentation system for automatic detection and localization of sea-ice formations from close-range optical images." *IEEE Sensors Journal* 21.16 (2021): 18004-18019.

57. Lu, Peng, and Zhijun Li. "A method of obtaining ice concentration and floe size from shipboard oblique sea ice images." *IEEE Transactions on geoscience and remote sensing* 48.7 (2010): 2771-2780.

58. “CCGS Amundsen.” *Wikipedia*, 3 Feb. 2022, en.wikipedia.org/wiki/CCGS_Amundsen.

59. Transport Canada. 2019. Guidelines for assessing ice operational risk, TP NO. 15383E. March 2019

60. Timco, G. W., Ivana Kubat, and Michelle Johnston. "Scientific basis for the Canadian ice regime system." *18th International Conference on Port and Ocean Engineering under Arctic Conditions, Potsdam, NY, USA*. 2005.

61. Government of Canada 2017. Arctic shipping safety and pollution prevention regulations. SOR/2017–286.

62. Browne, Thomas, et al. "A method for evaluating operational implications of regulatory constraints on Arctic shipping." *Marine Policy* 135 (2022): 104839.

63. Kubat, Ivana, et al. "A methodology to evaluate Canada's Arctic shipping regulations." *International Conference on Port and Ocean Engineering under Arctic Conditions (POAC)*. 2005.

64. Transport Canada. "TP 12259E - Arctic Ice Regime Shipping System (AIRSS) Standard." *Transport Canada*, 26 Mar. 2018, tc.canada.ca/en/marine-transportation/marine-safety/tp-12259e-arctic-ice-regime-shipping-system-airss-standard. Accessed 20 Nov. 2024.

65. Tikka, Kirsi, Kaj Riska, and Shewen Liu. "Tanker design considerations for safety and environmental protection of Arctic waters: Learning from past experience." *WMU Journal of Maritime Affairs* 7 (2008): 189-204.

66. Fedi, Laurent, Olivier Faury, and Laurent Etienne. "Mapping and analysis of maritime accidents in the Russian Arctic through the lens of the Polar Code and POLARIS system." *Marine Policy* 118 (2020): 103984.

67. Kum, Serdar, and Bekir Sahin. "A root cause analysis for Arctic Marine accidents from 1993 to 2011." *Safety science* 74 (2015): 206-220.

68. Sonka, Milan, Vaclav Hlavac, and Roger Boyle. *Image processing, analysis and machine vision*. Springer, {2013}.

69. Dubrofsky, Elan. "Homography estimation." *Diplomová práce. Vancouver: Univerzita Britské Kolumbie* 5 (2009).

70. Ammar Abbas, Syed, and Andrew Zisserman. "A geometric approach to obtain a bird's eye view from an image." *Proceedings of the IEEE/CVF international conference on computer vision workshops*. 2019.

71. Sandru, Andrei, et al. "A complete process for shipborne sea-ice field analysis using machine vision." *IFAC-PapersOnLine* 53.2 (2020): 14539-14545.

72. Amundsen Science. *CCGS Amundsen Ship and Laboratories Plans*. amundsenscience.com/wp-content/uploads/2024/03/Ship-plans.pdf. Accessed 20 Nov. 2024.
73. BBC Science Focus. “How Far Away Is the Horizon?” *Www.sciencefocus.com*, www.sciencefocus.com/planet-earth/how-far-away-is-the-horizon.
74. American Bureau of Shipping. *Vessel Maneuverability*. 2006. Accessed 10 June 2024.
75. Sung, Young Jae, and Key-Pyo Rhee. "New prediction method on the stopping ability of diesel ships with fixied pitch propeller." *International shipbuilding progress* 52.2 (2005): 113-128.
76. Xie, Yaofeng, et al. "Research on berthing capability and working property of pontoon bases." *Journal of Coastal Research* 73 (2015): 505-510.
77. Papanikolaou, Apostolos, et al. "Simulation of the maneuvering behavior of ships in adverse weather conditions." *Proceedings*. 2016.
78. Pallis, Petros L. "Port risk management in container terminals." *Transportation research procedia* 25 (2017): 4411-4421.
79. Charchalis, Adam. "Dimensional constraints in ship design." *Journal of KONES* 20 (2013).
80. Jeong, Seong-Yeob, et al. "Prediction of ship resistance in level ice based on empirical approach." *International Journal of Naval Architecture and Ocean Engineering* 9.6 (2017): 613-623.
81. Imson, Grace. “How to Calculate the Distance to the Horizon: Easy Formulas.” WikiHow, 23 May 2005, *www.wikihow.com/Calculate-the-Distance-to-the-Horizon*. Accessed 17 Feb. 2025.
82. Zhan, Dexin, et al. "Numerical simulation of ship maneuvering in pack ice." *International Conference on Offshore Mechanics and Arctic Engineering*. Vol. 49125. 2010.
83. Huang, Luofeng, et al. "Ship resistance when operating in floating ice floes: A combined CFD&DEM approach." *Marine Structures* 74 (2020): 102817.

84. Browne, Thomas, et al. "A framework for integrating life-safety and environmental consequences into conventional arctic shipping risk models." *Applied Sciences* 10.8 (2020): 2937.

85. Browne, Thomas, et al. "Consequence modelling for Arctic ship evacuations using expert knowledge." *Marine Policy* 130 (2021): 104582.

Appendix A

Matlab Scripts Used in Manoeuvrability Calculations

1. Method 1 Stopping Distance

```
vesselname = A;
vessel_type = ["VLCC";"Cargo Ship";"Cargo Ship";"Ferry";"Cargo
Ship";"Tanker";"Tanker";"Ferry"];
vessel_engine = "Diesel";
vessel_L = [350; 98; 189; 200; 210; 271; 292; 85];            %L
x = 8;
vessel_Vs   = [x; x; x; x; x; x; x; x];     %vessel test speed (knots)
vessel_TRv = 195; %%using 120s, 300s and 540s  ##Used time of 195s after
calibrating with results from the ABS Guide

%type of engine [Steam or Diesel]  and vessel type [Gas Carrier, VLCC, Cargo
Ship, Ferry or Tanker]
%vessel length (m), vessel time to reverse (sec), vessel speed (knots) TODO:
Determine how the time is calculated
  % This file will calculate the head reach of a vessel given its length and
other parameters
    %Parameters
    %vessel_CL %vessel coefficient that depends on length
    %vessel_TRv %time in seconds to achieve reverse thrust
    %vessel_Vs %vessel cruise speed
    %vessel_C %coefficient dependent on the product of time taken to achieve the
astern thrust and initial speed
    %vessel_BLow %low boundary for coefficient dependent on vessel resistance
    %vessel_BHigh %high boundary for coefficient dependent on vessel resistance
    %vessel_ALow %low coefficient dependent on mass of vessels
    %vessel_AHigh %high coefficient dependent on mass of vessels
    %Vessel_SLow %low boundary for stopping distance
    %vessel_SHigh %high boundary for stopping distance

%Outputs
len = length(vessel_L);
vessel_C = zeros(len, 1);
vessel_CL = zeros(len, 1);
vessel_SLow = zeros(len, 1);
vessel_SHigh = zeros(len, 1);
vessel_ALow = zeros(len, 1);
vessel_AHigh = zeros(len, 1);
vessel_BLow = zeros(len, 1);
vessel_BHigh = zeros(len, 1);

for i = 1:len
    %Equation for vessel_CL
    if vessel_L(i) <= 100
        vessel_CL(i)= 2.3;
    elseif vessel_L(i) <= 200
```

```
        vessel_CL(i) = -(0.012*vessel_L(i))+3.5;
    elseif vessel_L(i) <=300
        vessel_CL(i) = -(0.003*vessel_L(i))+1.7;
    else
        vessel_CL(i) = 0.8;
    end

    %Equation for vessel_C
           if vessel_Vs(i)<15
            vessel_C(i) = vessel_CL(i);
        elseif vessel_Vs(i)>(0.25*vessel_TRv)
            vessel_C(i) = vessel_CL(i)*(vessel_Vs(i)/15);
        elseif vessel_Vs <= 0.25*vessel_TRv
            vessel_C(i) = vessel_CL(i)*(vessel_TRv/60);
        else
            disp("The value for the calculation of C did not meet any of the
criteria in its definitios and thus could not be defined")
            vessel_C(i)=0;
        end

    %equations for the vessel_BLow and vessel_BHigh
    if vessel_engine=="Diesel"
        vessel_BLow(i)= 0.6;
        vessel_BHigh(i) = 1.0;
    elseif vessel_engine=="Steam"
        vessel_BLow(i) = 1.0;
        vessel_BHigh(i) = 1.5;
    else
        print("The specified vessel engine must either be Diesel or Steam. Other
types are not factred in this calculation")
        vessel_BLow(i) = 0;
        vessel_BHigh(i) = 0;
    end

    %Equations for the calculation of vessel_ALow and vessel_AHigh
    if vessel_type(i)=="Cargo Ship"
        vessel_ALow(i)= 5;
        vessel_AHigh(i) = 8;
    elseif vessel_type(i)=="Ferry"
        vessel_ALow(i) = 8;
        vessel_AHigh(i) = 9;
    elseif vessel_type(i)=="Gas Carrier"
        vessel_ALow(i)= 10;
        vessel_AHigh(i) = 11;
    elseif vessel_type(i)=="Tanker"
        vessel_ALow(i) =12;
        vessel_AHigh(i)= 13;
    elseif vessel_type(i)=="VLCC"
        vessel_ALow(i) = 14;
        vessel_AHigh(i) = 16;
    else
        disp("The specified type of vessel is not supported in this calculation")
        vessel_ALow(i) = 0;
        vessel_AHigh(i) = 0;
    end
```

```
    %Equation for the stopping distance
    vessel_SLow(i) = (vessel_ALow(i)*(log10(1+vessel_BLow(i))))+vessel_C(i);
    vessel_SHigh(i) = (vessel_AHigh(i)*(log10(1+vessel_BHigh(i))))+vessel_C(i);
end
```

2. Method 2 Stopping Distance

```
%Prarameters
A = ["Sample ABS Vessel";"Amundsen";"Umiak";"Blue Puttees";"Connaigra";"MV
Mattea";"Terra Nova";"Atlantic Kestrel"];
vesselname = A;
x = 3;

%%Inputs
vessel_mass = [355600000.0; 5911000; 22462000; 28460000; 26800000; 76216000;
193000000; 6186000]*0.001;              %m  kg
surge_speed = [x; x; x; x; x; x; x; x]*0.514;        %V m s^-1
approach_Speed =[x; x; x; x; x; x; x; x]*0.514;     %V0 m s^-1
coasting_Speed = x*0.8*0.514;     %Vc m s^-1
vessel_L = [350; 98; 189; 200; 210; 271; 292; 85];            %L
vessel_B = [58.3; 19.5; 26.6; 26.7; 29.6; 45.0; 45.5; 22.0];
vessel_T = [19.4; 7.2; 11.7; 6.2; 8.6; 9.4; 9.5; 8.0];
Speed_MCR  = [15; 15; 14; 22; 24; 20; 8; 15];           %V_MCR knots
BHP_MCR   = [30000; 13600*6; 29171; 14685; 22842; 25390; 33500; 16094];       %
propeller_RPM  =82.0;       %nC
vessel_TRv = 3.5*60; %%using 120s, 300s and 540s

%alpha_con                   %a
%surge_mass                  %mx kg
%wetted_surface_con          %S
%skin_coeff                  %k'
%astern_Thrust               %Ts
%approach_S_Resistance       %R0
%coasting_Distance           %Sc
%Thrust_MCR                  %T_MCR
%DHP_MCR                     %
%wake_fraction               %w

%constants
ratio_Thrust = 0.75;         %
water_density = 1025.0;      %p  kg/m^3
water_viscosity = 0.00000104;
open_water_eff = 0.65;       %no
relative_rotation_eff = 1.0;%nR
alpha_con = 0.5;

%%Outputs
len = length(vessel_L);
stop_Distance = zeros(len,1);
ship_length = zeros(len,1);
volume_displacement = zeros(len,1);
reynolds_N = zeros(len,1);
```

```
Block_coeff = zeros(len,1);
wake_fraction = zeros(len,1);
Thrust_MCR = zeros(len,1);
astern_Thrust = zeros(len,1);
wetted_surface_con = zeros(len,1);
skin_coeff = zeros(len,1);
approach_S_Resistance = zeros(len,1);
coasting_J = zeros(len,1);
coasting_Distance = zeros(len,1);
A_term = zeros(len,1);
B_term = zeros(len,1);
C_term = zeros(len,1);

for i = 1:len

volume_displacement(i) = vessel_mass(i)/water_density; % m^3
reynolds_N(i) = vessel_L(i)*surge_speed(i)/water_viscosity;   %Rn
Block_coeff(i) = volume_displacement(i)/(vessel_L(i)*vessel_B(i)*vessel_T(i));
%CB

surge_mass = 0.08*vessel_mass(i);
wake_fraction(i) = (0.5*Block_coeff(i))-0.05;
DHP_MCR = 0.99*BHP_MCR(i);
Thrust_MCR(i) = 745.7*open_water_eff*relative_rotation_eff*DHP_MCR/((1-
wake_fraction(i))*Speed_MCR(i));
astern_Thrust(i) = ratio_Thrust*Thrust_MCR(i);
wetted_surface_con(i) =
(volume_displacement(i)^(2/3))*3.4*vessel_L(i)/(2*volume_displacement(i)^(1/3));
skin_coeff(i) = 0.463*(log10(reynolds_N(i))^-2.6)*((4.5*Block_coeff(i))-1.4);
approach_S_Resistance(i) = (water_density/2)*wetted_surface_con(i)*skin_coeff(i);
coasting_J(i) = (1-wake_fraction(i))/(coasting_Speed*propeller_RPM*vessel_T(i));
%coasting_Speed = coasting_J*propeller_RPM*captal_D/(1-wake_fraction);
coasting_Distance(i) = (((vessel_mass(i) +
surge_mass)*approach_Speed(i)^2)/(approach_S_Resistance(i)-
(alpha_con*(approach_Speed(i)^2))))*log10(approach_Speed(i)/coasting_Speed);
A_term(i) = ((vessel_mass(i) +
surge_mass)*((approach_Speed(i)^2)/(2*approach_S_Resistance(i)*vessel_L(i))));
B_term(i) = (approach_S_Resistance(i)/astern_Thrust(i));
C_term(i) = 0.5*approach_Speed(i)*vessel_TRv/vessel_L(i);

ship_length(i) = ((A_term(i)*log10(1+B_term(i)))+C_term(i));
stop_Distance(i) = ship_length(i)*vessel_L(i);
end
```

3. Turning Circle Advance and Transfer

```
%Turning_Circle
A = ["Sample ABS Vessel";"Amundsen";"Umiak";"Blue Puttees";"Connaigra";"MV
Mattea";"Terra Nova";"Atlantic Kestrel"];
vesselname = A;
Speed = 8; %knots
x = Speed;
```

```
%Inputs
vessel_L    = [350; 98; 189; 200; 210; 271; 292; 85];      %vessel length
vessel_B    = [58.3; 19.5; 26.6; 26.7; 29.6; 45.0; 45.5; 22.0];     %vessel molded
breadth
vessel_T    = [19.4; 7.2; 11.7; 6.2; 8.6; 9.4; 9.5; 8.0];      %design draft at
full load (m)  ##TODO
vessel_TL   = [19.4; 7.2; 11.7; 6.2; 8.6; 9.4; 9.5; 8.0]*0.75;      %draft at
which turning circle is estimatedin (m)  ##TODO
vessel_Vs   = [x; x; x; x; x; x; x; x];     %vessel test speed (knots)
vessel_mass = [355600000.0; 5911000; 22462000; 28460000; 26800000; 76216000;
193000000; 6186000];             %m  kg

%constants
water_density = 1025.0;     %p  kg/m^3
theta_R     = 45;  %rudder angle
trim        = 0.85;          %static trim in (m) ##TODO
vessel_Sp   = 15.2;         %span of rudder (m)  ##TODO
vessel_Ch   = 10.8;         %mean chord of rudder (m)  ##TODO
vessel_ST   = 1.0;          %vessel stern type  ##TODO
vessel_Ab   = 8.0;          %submerged area (m)  ##TODO

%outputs
len = length(vessel_L);
advance = zeros(len,1);
transfer = zeros(len,1);
vessel_Cb = zeros(len,1);
vessel_STD = zeros(len,1);
vessel_TD = zeros(len,1);

for i = 1:len

    volume_displacement = vessel_mass(i)/water_density; % m^3
    vessel_Cb(i)   = volume_displacement/(vessel_L(i)*vessel_B(i)*vessel_T(i));
%CB;     %block coefficient

%Calculations
vessel_STD(i) = 4.19-(203*(vessel_Cb(i)/theta_R)) + 47.4*(trim/vessel_L(i)) -
(13.0*(vessel_B(i)/vessel_L(i))) + (194/theta_R) -
((35.8*vessel_Sp*vessel_Ch/(vessel_L(i)*vessel_T(i)))*(vessel_ST-1)) +
((3.82*vessel_Sp*vessel_Ch/(vessel_L(i)*vessel_T(i)))*(vessel_ST-2)) +
(7.79*vessel_Ab/(vessel_L(i)*vessel_T(i))) + 0.7*((vessel_T(i)/vessel_TL(i))-
1)*(theta_R/(abs(theta_R)))*(vessel_ST-1);

vessel_TD(i) =
((0.910*vessel_STD(i))+(0.424*vessel_Vs(i)/(sqrt(vessel_L(i))))+0.675);
advance(i) = (0.519*vessel_TD(i))+1.33;
transfer(i) = (0.497*vessel_TD(i))-0.065;

end


% T = table(vesselname, vessel_L, vessel_B, vessel_T, vessel_Vs, advance, transfer);
% filename = 'New Method 3 ABS Advance and Transfer.xlsx';
% writetable(T,filename,'Sheet','Stopping_Distances','Range','B2');
```

```
disp(transfer)%.*vessel_L)
disp(advance)%.*vessel_L)
```

Appendix B

Image Processing Scripts

1. Greyscale Conversion and Contrast Enhancement

```
current_img = imread("Rotated Sample Image for Thesis.jpg");
I_b = rgb2gray(current_img);

I_imadjust = imadjust(I_b);
I_histeq = histeq(I_b);
I_adapthisteq = adapthisteq(I_b);

% imshow(I_show)
I_temp= I_imadjust;
montage({current_img,I_b,I_imadjust},"Size",[1 3])
title("Original Image, Greyscale and Enhanced Image")
```

2. Camera Lens distortion Removal

```
%Link: https://www.mathworks.com/help/vision/ref/undistortimage.html
%Distortion theory: https://www.mathworks.com/help/visionhdl/ug/image-
undistort.html

images = imageDatastore(fullfile(toolboxdir('vision'),'visiondata', ...
    'calibration','mono'));
%Script 2 for now

% images = imageDatastore("C:\Program
Files\MATLAB\R2023b\toolbox\vision\visiondata\calibration\mono");
[imagePoints,boardSize] = detectCheckerboardPoints(images.Files);
squareSize = 70;  %The square size is in millimeters.
worldPoints = generateCheckerboardPoints(boardSize,squareSize);
I = I_temp;
imageSize = [size(I,1),size(I,2)];
cameraParams = estimateCameraParameters(imagePoints,worldPoints, ...
                                  'ImageSize',imageSize);
J1 = undistortImage(I,cameraParams);
%I = readimage(images,1);
figure; imshowpair(I_temp,J1,'montage');
title('Original Image (left) vs. Corrected Image (right)');

I_temp = J1;
```

3. Projective Transformation Script

```
% % Homography matrix determination
image_temp = imread("Result 1 corrected fisheye size.png");

%Inputs
% From cameraParams
%  K = [892.140926181639     0     615.568291022080
% 0 896.126984179547    317.815103380409
% 0 0      1]

% I_temp = J1;
I_temp = image_temp;
% I_temp = undistortedImage;

theta = 60;  %in degrees
fx = 892;
fy = 896;
Sx = 1.0;
Sy = 1.0;
cx = 615.5;
cy = 317;

% First determine the rotation matrix R
R = [1 0 0 ;
    0 cosd(theta) -sind(theta);
    0 sind(theta) cosd(theta)]
%Second we determine the camera intrinsic matrix K
K = [fx/Sx 0 cx;
    0 fy/Sy cy;
    0 0 1]
K_inv = inv(K);

%Now to find the homography matrix

H_temp = R*K_inv; %alternative suggestion to use H = K*R\K
H = K*H_temp;
I = I_temp;
I_bnw = im2gray(I);
imshow(I_bnw)
tform = projective2d(H');
J = imwarp(I_bnw,tform);
figure
imshow(J)

I_temp = J;
```

4. Image Rescaling Script

```
% Step 1: Read the image
% img = imread('Input for Step 5.jpg'); % Replace with your image file
img = imread('Sample for stretch edit.jpg'); % Replace with your image file
[m, n, c] = size(img); % Get the dimensions of the original image
% scales = xlsread("Research calculation Images.xlsx","Image Points
Calculations","E2:E380");
```

```
% save("scales2.mat","scales");

%Scales
load scales2.mat
scales = scales/100;

% roundn = @(x,n) round(x*10^n)./10^n;
% scales = roundn(scales,2);

% n = 2;
% roundn = @(x,n) round(x*10^n)./10^n;
% x2 = roundn(x,2)
% fun3 = @(x) sprintf('%0.2f', x2);
% x3 = fun3(x2)

%Inputs
%600 to 220
%
res = 2; %code runs out of memory at scale of 5
scales = scales *res;
BottomL = 600;
TopL = 220;
iniCount = TopL+1;

Myscales= round(scales); %(BottomLmain-BottomL:BottomLmain-TopL);  %
xlsread("Research calculation Images.xlsx","Image Points
Calculations","E51:E75"); %%to adjust cell range
Revmyscales=flip(Myscales);
TRevmyscales=Revmyscales';
filler = ones(1,(m-(BottomL)));
filler2 = ones(1,(TopL))*TRevmyscales(1);
finalScale = cat(2,filler2,TRevmyscales,filler);

V = round(finalScale);
Gray_Img = rgb2gray(img);
M = im2single(Gray_Img);

% % Define the initial matrix
% M = [7 7 0,
%      0 5 0,
%      0 3 0];
%
% % Define the vector
% V = [3, 2, 2];  % Repetition factors for each row

%% Section 1: Replicating each element within the row by its scale factor

% Initialize an empty cell array to hold the expanded rows

max_Factor = max(finalScale);
expandedRow = repelem(M(iniCount,:),1, V(iniCount));
maxLen = size(expandedRow,2);

combinedArray = zeros(size(M,1), maxLen);
combinedArray(1,:) = expandedRow;
```

```
% Loop through each row in the matrix
for i = 1:(size(M, 1)-iniCount-1)
    % Repeat the row V(i) times (expand rows)
    expandedRow = repelem(M(i+iniCount,:),1, V(i+iniCount));
    currentLen = length(expandedRow);

        % Calculate the number of zeros needed on both sides
    totalPadding = maxLen - currentLen;
    leftPadding = floor(totalPadding / 2);  % Zeros to add on the left
    rightPadding = ceil(totalPadding / 2);  % Zeros to add on the right

    % Create a new row with the vector padded symmetrically
    combinedArray(i+1, :) = [zeros(1, leftPadding), expandedRow, zeros(1,
rightPadding)];
    disp(i);

    % % % Expand each element within the row by 3 times (expand columns)
    % % expandedRow = repelem(expandedRow, 1, 4)
    % %
    % % % Store the expanded row(s) in the cell array
    % % expandedRows = [expandedRows; mat2cell(expandedRow, ones(V(i), 1),
size(expandedRow, 2))]
end

%% Section 2: Replicating Each Row By its Scale Factor

% Initialize an empty cell array to hold the expanded rows
% V = round(V/res);
offset = 0; %For further image analysis
startindex = (iniCount+offset);
endindex = size(V,2);
ExpandedRows = {};

% Loop through each row in the matrix
for j = 1:(size(combinedArray, 1)-1)
    % Repeat the row V(i) times (expand rows)
    ExpandedRow = repmat(combinedArray(j,:), V(j), 1);

    % Store the expanded row(s) in the cell array
    ExpandedRows = [ExpandedRows; mat2cell(ExpandedRow, ones(V(j), 1),
size(ExpandedRow, 2))];
    disp(j)
end

%%
% Concatenate all expanded rows into the final matrix
M_expanded = cell2mat(ExpandedRows);

% Display the final expanded matrix
% disp(M_expanded);
imshow(M_expanded)


%%
```

```
% Display the final combined array
% % disp(combinedArray);

% % Concatenate all expanded rows into the final matrix
% % M_expanded = cell2mat(expandedRows);
% %
% % % Display the final expanded matrix
% % disp(M_expanded);
```